© 2022. Published by The Company of Biologists Ltd | Journal of Cell Science (2022) 135, jcs259297. doi:10.1242/jcs.259297

RESEARCH ARTICLE

Hedgehog pathway modulation by glypican 3-conjugated heparan sulfate

Yulu Cherry Liu[1,2,*], Bradley M. Wierbowski[1] and Adrian Salic[1,*]

ABSTRACT

Glypicans are a family of cell surface heparan sulfate proteoglycans that play critical roles in multiple cell signaling pathways. Glypicans consist of a globular core, an unstructured stalk modified with sulfated glycosaminoglycan chains, and a glycosylphosphatidylinositol anchor. Though these structural features are conserved, their individual contribution to glypican function remains obscure. Here, we investigate how glypican 3 (GPC3), which is mutated in Simpson–Golabi–Behmel tissue overgrowth syndrome, regulates Hedgehog signaling. We find that GPC3 is necessary for the Hedgehog response, surprisingly controlling a downstream signal transduction step. Purified GPC3 ectodomain rescues signaling when artificially recruited to the surface of GPC3-deficient cells but has dominant-negative activity when unattached. Strikingly, the purified stalk, modified with heparan sulfate but not chondroitin sulfate, is necessary and sufficient for activity. Our results demonstrate a novel function for GPC3-associated heparan sulfate and provide a framework for the functional dissection of glycosaminoglycans by *in vivo* biochemical complementation.

This article has an associated First Person interview with the first author of the paper.

KEY WORDS: Signaling, Glycosaminoglycans, Heparan sulfate, Glypican, Hedgehog

INTRODUCTION

Glypicans (GPCs) are a family of cell surface heparan sulfate proteoglycans (HSPGs) deeply implicated in embryogenesis, adult physiology and disease (Selleck, 1999; Filmus et al., 2008; Sarrazin et al., 2011). GPCs were initially biochemically identified as a class of glycosylphosphatidylinositol (GPI)-anchored cell surface HSPGs, comprising a characteristic 64-kDa core protein (de Boeck et al., 1987; David et al., 1990). Subsequent molecular genetic studies revealed that vertebrates contain six GPC paralogs, GPC1 to GPC6 (Filmus et al., 2008). Although the six GPCs diverge considerably in primary sequence, they share a conserved domain architecture, consisting of a globular N-terminal cysteine-rich domain (Kim et al., 2011; Pei and Grishin, 2012; Svensson et al., 2012), followed by a flexible C-terminal stalk, which hosts multiple Ser-Gly attachment sites for sulfated glycosaminoglycan (GAG) chains (Bourdon et al., 1987), and ending with the terminal GPI anchor, which is embedded in the membrane. All vertebrate GPCs are important regulators of cell growth and embryonic development. GPC1 and GPC2 are required for brain development (Stipp et al., 1994; Jen et al., 2009). GPC3, perhaps the best characterized vertebrate GPC, is mutated in Simpson–Golabi–Behmel syndrome, a disorder characterized by tissue overgrowth, and renal medullary dysplasia with cyst formation (Pilia et al., 1996; Shi and Filmus, 2009), phenotypes that are recapitulated by mouse models of GPC3 loss (Cano-Gauci et al., 1999; Grisaru and Rosenblum, 2001; Chiao et al., 2002). GPC4 is involved in cell polarity during embryonic convergent extension (Topczewski et al., 2001) and craniofacial development (LeClair et al., 2009). GPC5 is implicated in cancer (Li et al., 2011) and kidney diseases (Grisaru and Rosenblum, 2001; Roberts and Gleadle, 2008; Okamoto et al., 2011, 2015), and GPC6 is important in bone development (Campos-Xavier et al., 2009; Capurro et al., 2017).

Much of the present thinking about GPC function derives from genetic studies of the two *Drosophila* GPCs, Division abnormally delayed (Dally) (Nakato et al., 1995) and Dally-like protein (Dlp) (Khare and Baumgartner, 2000), which regulate several of the signaling pathways that orchestrate early metazoan development, including Decapentaplegic (Dpp) (Jackson et al., 1997; Belenkaya et al., 2004), Wingless (Wg)/Wnt (Lin and Perrimon, 1999; Tsuda et al., 1999; Baeg et al., 2001; Franch-Marro et al., 2005; Han et al., 2005), Hedgehog (Hh) (Desbordes and Sanson, 2003; Lum et al., 2003; Han et al., 2004b; Yao et al., 2006; Williams et al., 2010) and fibroblast growth factor (FGF) (Yan and Lin, 2007). Specifically, the *Drosophila* GPCs regulate both the spread of morphogens through embryonic tissues, as well as signaling responses in target cells, though the two paralogs differ in their mode of regulation within a given pathway, and in their requirement across different pathways and developmental contexts (Häcker et al., 2005).

In addition to the importance of individual GPCs, genetic studies have suggested a critical role for the attached GAG chains. In *Drosophila*, mutants in GAG biosynthetic enzymes, such as Sugarless (Binari et al., 1997; Häcker et al., 1997; Haerry et al., 1997), Tout-velu (Ttv) (Bellaiche et al., 1998) and its relatives, Botv and Sotv (Han et al., 2004a; Takei et al., 2004), and Sulfateless (Lin and Perrimon, 1999), exhibit developmental phenotypes overlapping with those caused by the loss of GPCs. Similarly, mutations in the heparan sulfate biosynthetic enzyme EXT1 causes hereditary multiple exostoses in humans (Ahn et al., 1995).

In spite of the striking developmental and disease phenotypes caused by impaired GPC function, their molecular basis has remained obscure. In particular, it is not known what accounts for the different activities of GPC paralogs. One possible explanation is that their GAG chains dictate context-specific interactions (Bülow and Hobert, 2006). Heparan sulfate, the primary class of GPC-attached GAGs, consists of a linear chain of repeating disaccharide units, which can be modified by epimerization and by sulfation of

[1]Department of Cell Biology, Harvard Medical School, Boston, MA 02115, USA. [2]Department of Biology, Hood College, Frederick, MD 21701, USA.

*Authors for correspondence (liuyc@hood.edu; adrian_salic@hms.harvard.edu)

Y.C.L., 0000-0003-4861-6915; B.M.W., 0000-0002-1967-5919; A.S., 0000-0002-0748-9545

Handling Editor: Guangshuo Ou
Received 19 August 2021; Accepted 4 February 2022

Journal of Cell Science (2022) 135, jcs259297. doi:10.1242/jcs.259297

four distinct sites, in combinatorial fashion. Moreover, the length of heparan sulfate chains, as well as the extent, type and pattern of their positional modification, can vary (Xu and Esko, 2014). Such structural differences could direct the interaction of a single GPC with multiple partners, an idea supported by the existence of ligand-specific heparan sulfate substructures, such as those involved in binding FGF2 (Turnbull et al., 1992).

Although considerable progress has been made in the structural characterization of GAG chains (Prabhakar et al., 2009), methods for the functional interrogation of specific GAG modifications have been limited. Genetic ablation of GAG-modifying enzymes in whole organisms (Townley and Bülow, 2011) or target cells (Esko et al., 1985) affect multiple proteoglycan classes, each including several family members. Similarly, mutagenesis of GAG attachment sites of a proteoglycan (Williams et al., 2010) addresses the effect of complete GAG loss, rather than that of discrete elements of GAG substructure.

In this study, we develop a genetic and biochemical approach for the precise functional interrogation of GAG substructure, focusing on the role of GPC3 (Pilia et al., 1996; Cano-Gauci et al., 1999; Shi and Filmus, 2009) in cell signaling. GPC3 has been implicated in both Hh and Wnt signaling (De Cat et al., 2003; Capurro et al., 2005; Song et al., 2005; Capurro et al., 2008; Li et al., 2011; Filmus and Capurro, 2014; Capurro et al., 2015; Holtz et al., 2015; Capurro et al., 2017; Kolluri and Ho, 2019), but the mechanism remains unknown. We find that GPC3 is necessary specifically for Hh signaling but not Wnt signaling. Surprisingly, GPC3 does not affect the initial steps involved in vertebrate Hh pathway activation, which occur in primary cilia (Bangs and Anderson, 2017). Instead, the GPC3 requirement occurs downstream of ligand reception, at the level of Gli proteins, the transcriptional effectors of the Hh pathway (Aza-Blanc et al., 2000; Bai and Joyner, 2001). The purified ectodomain of GPC3, when recruited artificially to the cell surface of GPC3-deficient cells, rescues the Hh signaling defect. In contrast, the soluble unattached GPC3 ectodomain exhibits a dominant-negative effect on the Hh pathway. Using protein purified from a panel of cells defective in different GAG biosynthetic enzymes, we demonstrate that the GPC3 ectodomain activity requires heparan sulfate but not chondroitin sulfate. Strikingly, the heparan sulfate-modified unstructured stalk of GPC3 is sufficient to recapitulate the activity of the entire protein, with the rest of the GPC3 molecule dispensable. These results define a novel role for GPC3-derived heparan sulfate in Hh signaling, and outline a systematic biochemical complementation strategy for the functional dissection of GAG substructure.

RESULTS

GPC3 is necessary for Hh signaling

To test whether GPC3 is involved in the Hh pathway (Fig. 1A), we inactivated *Gpc3* in mouse embryonic fibroblasts (MEFs) (Fig. S1A), using CRISPR/Cas9 (Table S1) (Ran et al., 2013). We then measured the transcriptional response to Hh pathway stimulation, by assaying induction of the *Gli1* target gene (Tukachinsky et al., 2010). As shown in Fig. 1B, when *Gpc3*^{KO} cells were treated with Shh, which activates Hh signaling by inhibiting the patched1 (Ptch1) receptor, *Gli1* induction was significantly lower compared to wild-type cells. As GPC3 has been proposed to compete with Ptch1 for Shh (Capurro et al., 2008), we tested whether GPC3 and Shh interact. Contrary to previous observations (Capurro et al., 2008), we were unable to detect binding of Shh to GPC3 (Fig. 1C,D; Fig. S1B,C), and, furthermore, GPC3 did not compete with Ptch1 for binding to Shh (Fig. 1E; Fig. S1D), suggesting that the effects of GPC3 on Hh signaling are not at the level of the Shh-Ptch1 interaction. Consistent with this idea, *Gpc3*^{KO} cells showed a blunted response even when the Hh pathway was stimulated downstream of Ptch1 using smoothened agonist (SAG; Chen et al., 2002), a synthetic compound that directly activates Smo (Fig. 1B). These results indicate that GPC3 is necessary for maximal Hh pathway activation, at the level of Smo or downstream of it.

We next asked whether the GPC3 requirement is specific for the Hh pathway. Previous studies suggested that GPC3 is required for Wnt signaling (De Cat et al., 2003; Capurro et al., 2005; Song et al., 2005). To test this possibility, we treated cells with Wnt3A and measured expression of the Wnt pathway-specific target gene *Axin2*. We observed no difference in *Axin2* induction by Wnt3A between wild-type and *Gpc3*^{KO} cells (Fig. 1F), indicating that Wnt pathway activation is unaffected by the loss of GPC3; this result is also consistent with a recent report (Dubey et al., 2020). Taken together, these data demonstrate that GPC3 is required for Hh signaling but not Wnt signaling.

GPC3 is required for signaling downstream of Smo

We sought to determine more precisely where GPC3 acts in the Hh pathway, by examining the dynamics of key pathway components in the primary cilium (Fig. 1A), the subcellular site where the initial steps in Hh signal transduction occur in vertebrate cells. In the resting state of the Hh pathway, the Shh receptor Ptch1 is localized to the primary cilium, inhibiting Smo and ensuring its exclusion from the cilium. Upon binding Shh, Ptch1 is inhibited and removed from the cilium, whereas Smo becomes active and accumulates in the cilium (Rohatgi et al., 2007; Tukachinsky et al., 2016; Bangs and Anderson, 2017; Petrov et al., 2017). In *Gpc3*^{KO} cells, Ptch1 localization to cilia in the absence of stimulation and its Shh-dependent removal from cilia occur normally (Fig. 1G,H), as does activation-dependent accumulation of Smo in cilia (Fig. 1I,J). These results indicate that loss of GPC3 does not impair Ptch1 and Smo ciliary dynamics, suggesting that GPC3 might impinge on a downstream step in Hh signaling.

We next investigated whether loss of GPC3 affects the Gli proteins Gli2 and Gli3, the zinc finger transcriptional factors that function as effectors of the Hh pathway (Dahmane et al., 1997; Aza-Blanc et al., 2000; Bai and Joyner, 2001). In wild-type cells, active Smo leads to Gli2 and Gli3 activation, and accumulation at the tips of cilia (Kim et al., 2009; Tukachinsky et al., 2010; Wen et al., 2010). Strikingly, in *Gpc3*^{KO} cells, accumulation of Gli proteins at ciliary tips is severely impaired (Fig. 1K,L), suggesting that GPC3 is required for the coupling between active Smo and the downstream Gli proteins.

Finally, we examined the consequence of GPC3 loss on the Gli3 protein. In the absence of Hh stimulation, full-length Gli3 (Gli3FL) is processed into a shorter form (Gli3R), which functions as repressor of the transcriptional output of the Hh pathway. Upon Hh stimulation, Gli3R levels drop and the levels of the transcriptional activator Gli3FL increase, causing increased transcription of *Gli1* and accumulation of Gli1 protein. In *Gpc3*^{KO} cells, we found that Gli3R levels were reduced normally upon SAG stimulation (Fig. 1M), suggesting that the observed inhibition of Hh signaling is not due to repression through Gli3R.

Rescue of GPC3 knockout cells by purified protein complementation

To demonstrate specificity of the Hh signaling defect of *Gpc3*^{KO} cells, we first tried rescue experiments by expressing full-length

Journal of Cell Science (2022) 135, jcs259297. doi:10.1242/jcs.259297

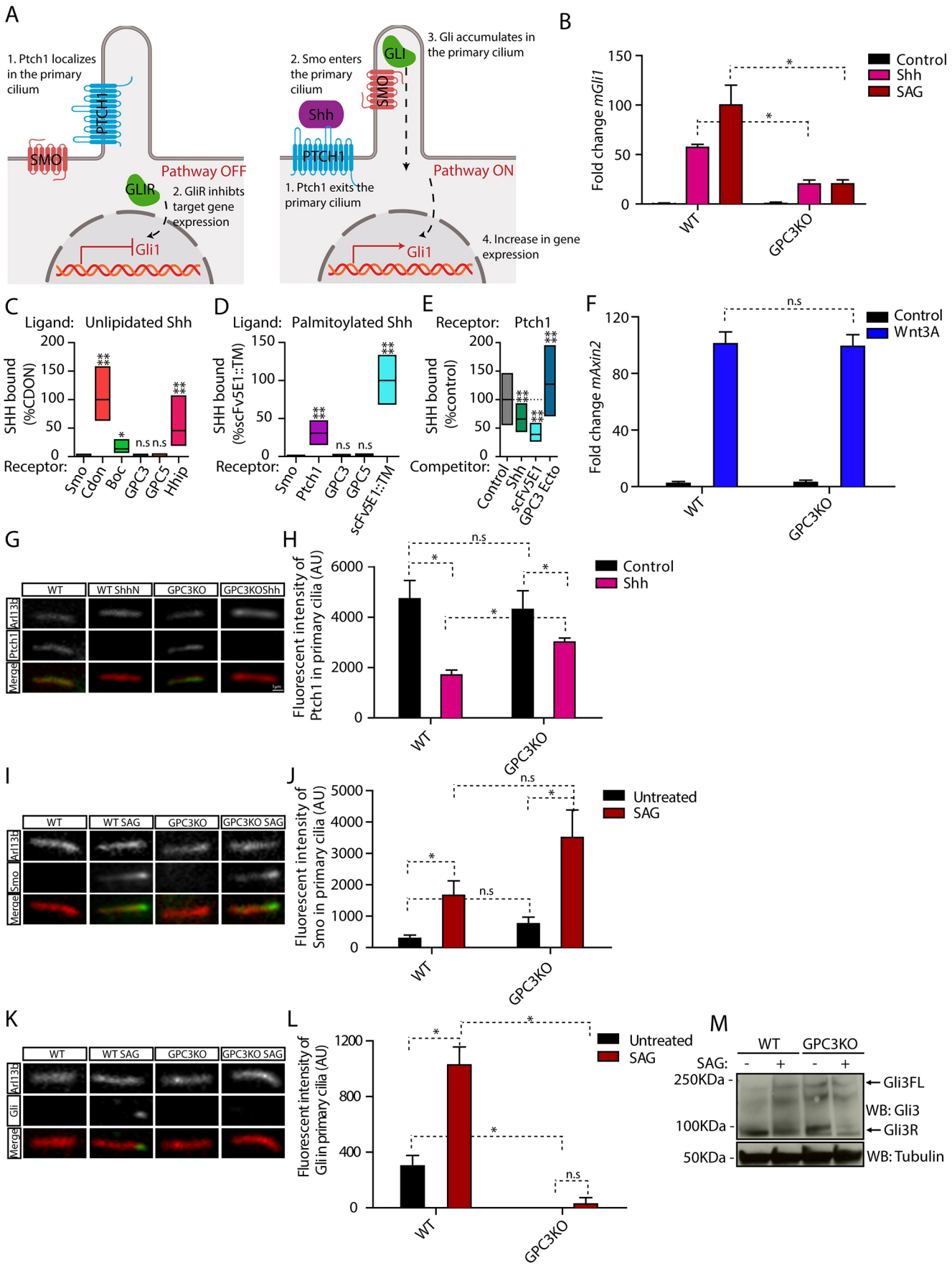

Fig. 1. See next page for legend.

Journal of Cell Science

Journal of Cell Science (2022) 135, jcs259297. doi:10.1242/jcs.259297

Fig. 1. Endogenous GPC3 is necessary for Hh pathway activation. (A) Schematic of the Hh pathway. Left: in the absence of signaling, Ptch1 in primary cilia inhibits Smo activation and localization to cilia. Right: upon pathway activation by Shh, Ptch1 is inhibited and exits from cilia, whereas Smo becomes active and accumulates in cilia. Smo activates Gli proteins, which accumulate at ciliary tips. Active Gli proteins turn on the transcriptional targets of the pathway, including *Gli1*. (B) Wild-type (WT) or *Gpc3*^{KO} MEFs were incubated with Shh, SAG (1 µM) or control medium for 24 h, and Hh signaling was measured by qRT-PCR for *Gli1*. Data are mean±s.e.m. of three replicates and were normalized from 0% (untreated) to 100% activation of the Hh pathway by saturating SAG. Hh pathway activation by Shh and SAG was significantly decreased in the absence of GPC3. (C) Fluorescently labeled unlipidated Shh was incubated with HEK293T cells transiently transfected with eGFP-tagged GPC3, GPC5 or control receptors, and bound ligand was quantified by fluorescence microscopy. Cdon, Boc and Hhip (left), as well as Ptch1 and a single-chain variant of the anti-Shh monoclonal antibody (scFv5E1) (Wierbowski et al., 2020) (right), were used as positive controls, and Smo was used as negative control. Data are normalized between binding to the negative control (0%) and the highest bound signal (100%). Boxplots represent the median and the first and third quartiles of binding. At least 200 cells were measured per condition. Neither GPC3 nor GPC5 binds unlipidated Shh. (D) As in C but using fluorescently labeled palmitoylated Shh. At least 1000 cells were measured per condition. Neither GPC3 nor GPC5 binds palmitoylated Shh. (E) As in C, except binding of palmitoylated Shh to Ptch1 was measured after preincubation of Shh with purified GPC3 ectodomain (GPC3-Ecto) or control competitors. Data are normalized between binding to Smo (negative control, 0%) and binding to Ptch1 in the presence of control competitor (100%). At least 1000 cells were measured per condition. GPC3-Ecto does not compete with Ptch1 for Shh binding. Shh binding was competed by scFv5E1 or by excess unlipidated Shh. (F) Wild-type or *Gpc3*^{KO} MEFs were incubated with Wnt3A-conditioned medium or control medium for 24 h, and Wnt signaling was measured by qRT-PCR for *Axin2*. Wnt pathway activation by Wnt3A was normal in the absence of GPC3. Data are mean±s.e.m. of three replicates. (G) Wild-type or *Gpc3*^{KO} MEFs stably expressing Ptch1-eGFP were incubated with Shh as in B, and ciliary intensity of Ptch1 was measured by immunofluorescence microscopy. Cilia were detected by staining for endogenous Arl13B. Ptch1 is green, Arl13B is red. In both wild-type and *Gpc3*^{KO} cells, Shh induces Ptch1 exit from cilia. (H) Quantification of the experiment in G. Data are mean±s.d. (300-400 cilia were measured per condition). (I) As in G but measuring ciliary levels of endogenous Smo following treatment with SAG (1 µM). Smo is green, Arl13B is red. In both wild-type and *Gpc3*^{KO} cells, SAG causes normal ciliary accumulation of Smo. (J) As in H but quantifying the experiment in I (300-400 cilia were measured per condition). (K) As in G but measuring ciliary intensity of endogenous Gli proteins. The anti-Gli antibody recognizes both full-length Gli2 and Gli3 (Tukachinsky et al., 2010). Gli is green, Arl13B is red. In the absence of GPC3, Gli proteins did not localize to the tips of cilia and their ciliary recruitment in response to SAG was greatly reduced. (L) As in H but quantifying the experiment in K (300-400 cilia were measured per condition). (M) As in B but cells were analyzed by immunoblotting for Gli3. Blotting for tubulin served as loading control. In the absence of GPC3, Gli3R was cleared normally by Hh pathway stimulation. Blots shown are representative of three experiments. **P*<0.05; *****P*<0.0001; n.s., not significant (two-tailed paired *t*-test). AU, arbitrary units. Scale bar: 1 µm (shown in G, also applies to I and K).

GPC3 (Fig. S1E,F). Although we could not establish MEF lines stably expressing full-length GPC3, transient transduction failed to reverse the defect (Fig. S1F); we speculate that this was due to non-physiological levels of GPC3 expression (Fig. S1G). Therefore, we turned to a purified protein complementation strategy for rescuing *Gpc3*^{KO} cells, which allows precise titration of the amount of added GPC3 (Fig. 2A). Briefly, the entire ectodomain of GPC3 was expressed and purified as a soluble secreted protein (GPC3-Ecto), tagged with the ALFA peptide at the C terminus (GPC3-Ecto-ALFA) (Fig. 2B). The ALFA peptide binds with sub-nanomolar affinity to the nanobody ALFA-NB (Gotzke et al., 2019), an interaction allowing the efficient recruitment of GPC3-Ecto-ALFA to the surface of cells expressing a membrane-anchored ALFA-NB (ALFA-NB::TM) (Fig. S2A); we used this system previously to recruit to the cell surface the ectodomain of GAS1, another GPI-anchored protein, like GPC3 (Wierbowski et al., 2020). When *Gpc3*^{KO} cells stably expressing ALFA-NB::TM were incubated with purified GAG-modified GPC3-Ecto-ALFA, we observed a dose-dependent rescue of recruitment of Gli proteins to primary cilia in response to Hh pathway stimulation (Fig. 2C); interestingly, too much GPC3-Ecto-ALFA was inhibitory (Fig. S2B). Importantly, GPC3-Ecto-ALFA rescued signal-dependent *Gli1* transcription in *Gpc3*^{KO} cells expressing ALFA-NB::TM (Fig. 2D,E). As expected, rescue was dependent on both ALFA tag and ALFA-NB::TM, as untagged GPC3-Ecto-ALFA did not rescue *Gpc3*^{KO} cells, and GPC3-Ecto did not rescue *Gpc3*^{KO} cells expressing ALFA-NB::TM. Together, these data demonstrate that the function of GPC3 in Hh signaling requires its membrane attachment, and, more generally, that surface recruitment of ectodomains is an efficient strategy for reconstituting glypican activity in cells, in a controlled manner.

Membrane-unattached GPC3 inhibits Hh signaling

In our rescue experiments, we noticed that purified GPC3-Ecto-ALFA inhibited Hh pathway activation in wild-type cells (Fig. 2E). This effect was also observed when wild-type cells were treated with purified GPC3-Ecto (Fig. 2E), or when GPC3-Ecto was expressed by viral transduction (Fig. S1F). Notably, GPC3-Ecto reduced the Hh response of wild-type cells to the levels of *Gpc3*^{KO} cells but did not further reduce signaling in *Gpc3*^{KO} cells (Fig. S1F); thus, the inhibitory activity of GPC3-Ecto requires endogenous GPC3. Taken together, these results suggest that GPC3-Ecto, when not membrane anchored, inhibits Hh signaling, perhaps by acting in dominant-negative fashion towards wild-type GPC3.

GAG modification is required for the effect of GPC3-Ecto in Hh signaling

We next investigated the requirements for the inhibitory activity of GPC3-Ecto on the Hh pathway. When affinity-purified GPC3-Ecto was subjected to size-exclusion chromatography, we noticed that it consisted of two pools: a broad high-molecular weight fraction, corresponding to GAG-modified protein (GPC3-Ecto^{GAG+}), and a defined monomeric species, corresponding to unmodified protein (GPC3-Ecto^{GAG-}) (Fig. 2B). To determine the role of GAG modification, we tested the effect of GPC3-Ecto^{GAG+} and GPC3-Ecto^{GAG-} on Hh signaling. Only GPC3-Ecto^{GAG+} inhibited pathway activation by Shh or SAG, with GPC3-Ecto^{GAG-} exhibiting inactivity (Fig. 3A). Similarly, constitutive Hh signaling that occurs in *Ptch1*$^{-/-}$ cells (Dahmane et al., 1997) was reversed by GPC3-Ecto^{GAG+} (Fig. S3A). Together, these results indicate that the GAG modification of GPC3 is critical for its effect on Hh signaling.

We performed a number of control experiments to assess the specificity of GPC3-Ecto^{GAG+} for the Hh pathway. We first investigated whether the effect is specific to GPC3 or is general to GAG-modified proteins. To address this, we purified the ectodomain of syndecan 1 (SDC1), a member of another class of cell surface HSPGs (Teng et al., 2012), and isolated the SDC1-Ecto^{GAG+} and SDC1-Ecto^{GAG-} fractions (Fig. S3B). Neither form of SDC1 had an effect on the Hh pathway response (Fig. S3C), confirming that the antagonistic effect is specific to GAG-modified GPC3. We also tested the effect of the different GPC3-Ecto forms on Wnt signaling. Neither GPC3-Ecto^{GAG+} nor GPC3-Ecto^{GAG-} had an effect on Wnt pathway transcriptional output, as measured by *Axin2* expression (Fig. S3D), consistent with the specificity of GPC3-Ecto^{GAG+} to the Hh pathway.

Journal of Cell Science (2022) 135, jcs259297. doi:10.1242/jcs.259297

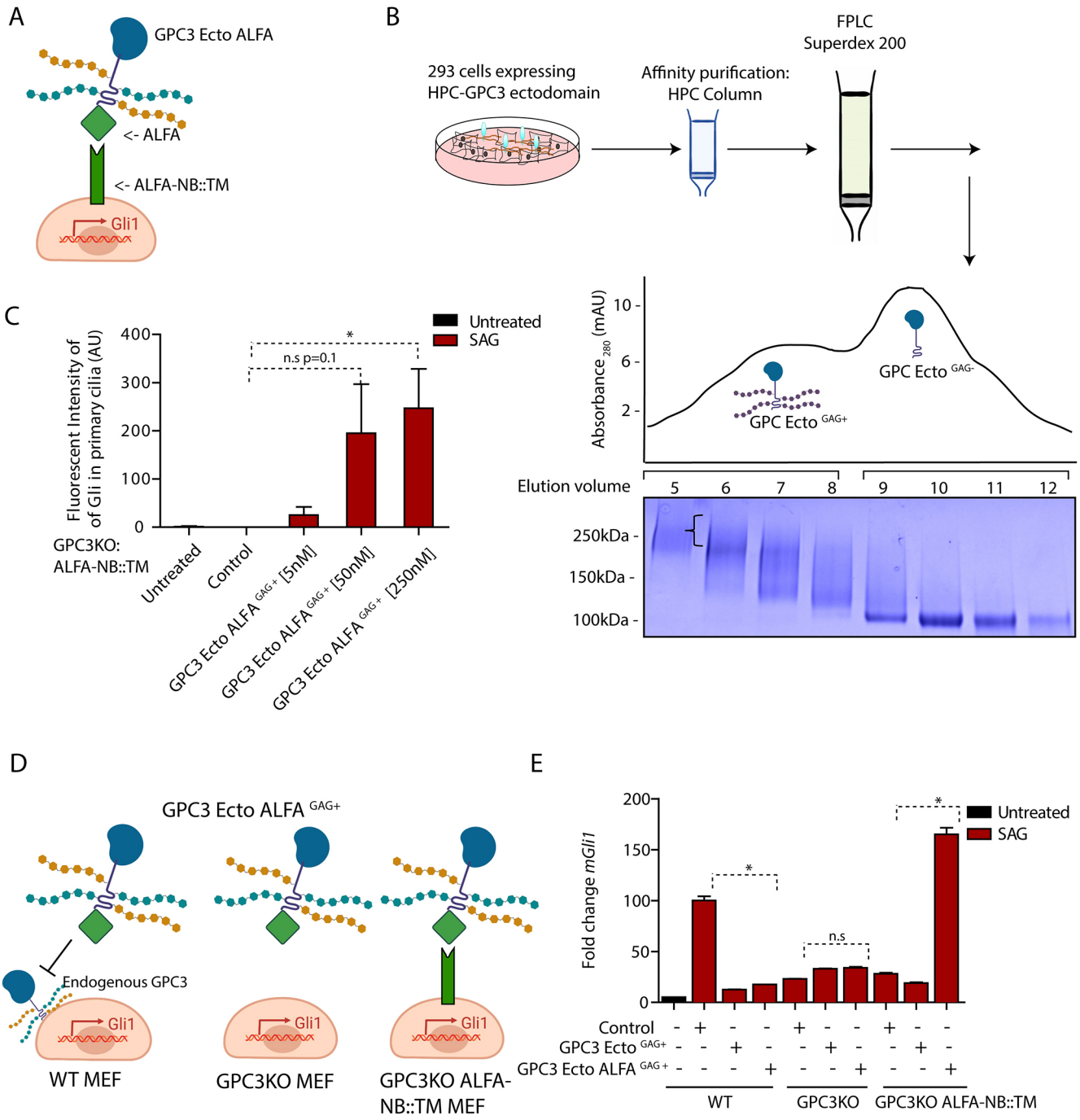

Fig. 2. Purified GPC3-GAG (+) recruited to the cell surface rescues loss of endogenous GPC3. (A) Cartoon illustration of *Gpc3*^{KO} MEFs expressing the membrane-bound ALFA nanobody (NB) construct ALFA-NB::TM, used to recruit GPC3-Ecto-ALFA to the cell surface. (B) Affinity-purified GPC3-Ecto fused to HaloTag was separated by size-exclusion chromatography to isolate GAG-modified and GAG-unmodified fractions. The indicated fractions were analyzed by SDS-PAGE and Coomassie staining. The bracket indicates the high molecular weight imparted by GAG modification of GPC3-Ecto. Gel shown is representative of three experiments. The *y* axis shows absorbance at 280 nm, expressed in mAU. (C) *Gpc3*^{KO} MEFs stably expressing ALFA-NB::TM were incubated with SAG (1 µM) for 6 h in the presence of the indicated concentrations of purified GPC3-Ecto-ALFA^{GAG+}. Ciliary intensity of endogenous Gli proteins was measured by immunofluorescence microscopy. Recruitment of GPC3-Ecto-ALFA^{GAG+} to the cell surface rescued signal-dependent accumulation of Gli at ciliary tips in a dose-dependent manner. Data are mean±s.d. (300-400 cilia were measured per condition). (D) Cartoon illustration of the experiment in E. (E) Wild-type (WT) MEFs, *Gpc3*^{KO} MEFs or *Gpc3*^{KO} MEFs stably expressing ALFA-NB::TM were incubated with SAG (1 µM) for 24 h in the presence or absence of 50 nM purified GPC3-Ecto-ALFA^{GAG+} or GPC3-Ecto^{GAG+}. Hh pathway output was measured by qRT-PCR for *Gli1*. Data are mean±s.e.m. of three replicates. Hh pathway activation is rescued when GPC3-Ecto-ALFA^{GAG+} is recruited to the cell surface. **P*<0.05; n.s., not significant (two-tailed paired *t*-test). AU, arbitrary units.

We further tested the idea that GPC3-Ecto^{GAG+} acts in a dominant-negative fashion by comparing its effects to those caused by GPC3 loss. Several results indicate that cells treated with purified GPC3-Ecto^{GAG+} behave like *Gpc3*^{KO} cells. GPC3-Ecto^{GAG+} had no effect on Shh-induced exit of Ptch1 from cilia (Fig. 3B), or Smo accumulation in cilia (Fig. 3C). Importantly, GPC3-Ecto^{GAG+} drastically reduced SAG-induced ciliary accumulation of Gli proteins (Fig. 3D), indicating that GPC3-Ecto^{GAG+} affects a step

Journal of Cell Science

Journal of Cell Science (2022) 135, jcs259297. doi:10.1242/jcs.259297

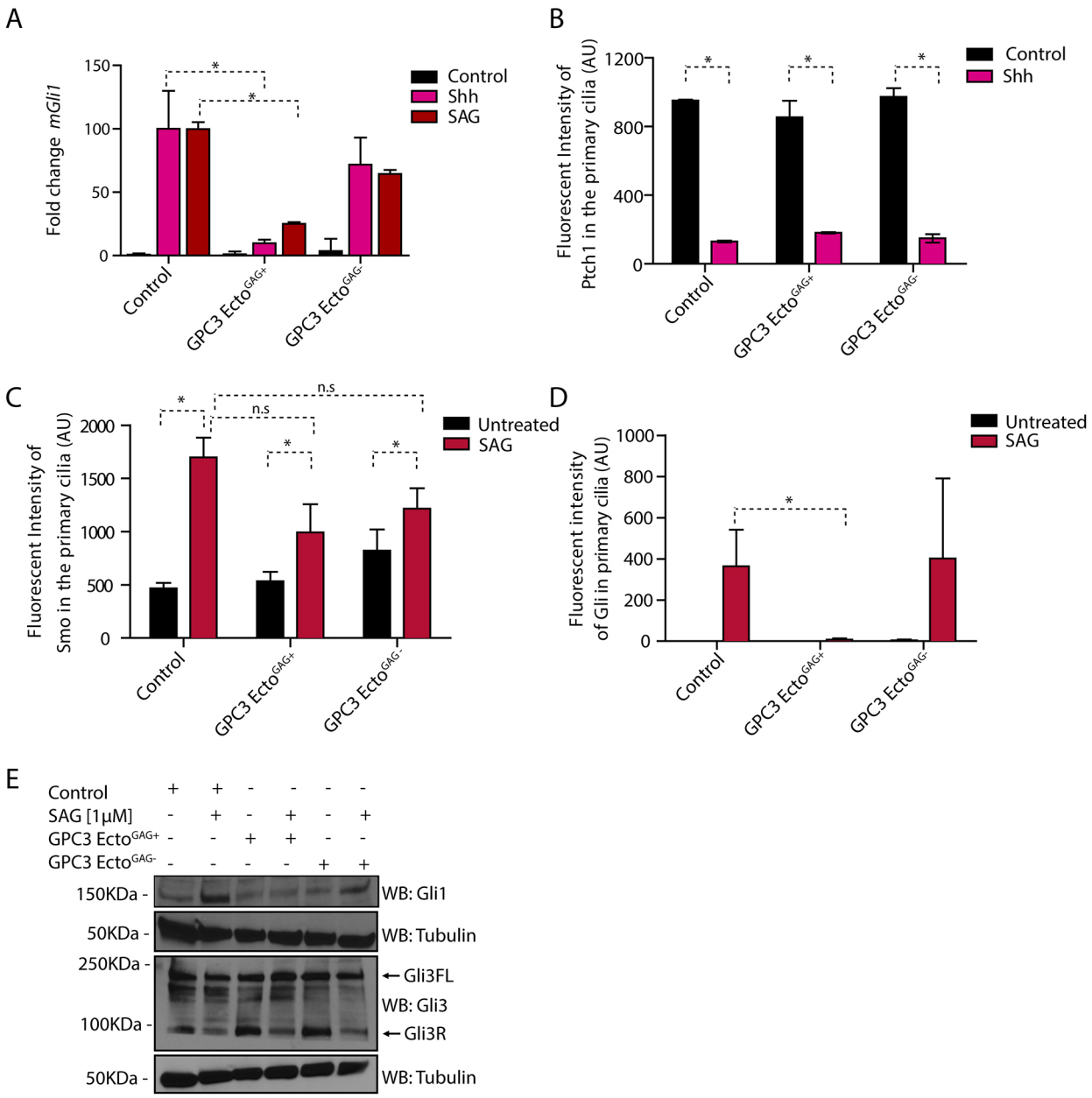

Fig. 3. Purified GPC3 ectodomain inhibits Hh signaling as dominant negative. (A) Wild-type MEFs treated with GPC3-Ecto^{GAG+} or GPC3-Ecto^{GAG-} were incubated with SAG (1 µM) or Shh for 24 h, and Hh pathway output was measured by qRT-PCR for *Gli1*. GPC3-Ecto^{GAG+} inhibits Hh signaling in wild-type MEF cells. Data are mean±s.e.m. of three replicates. (B) Wild-type MEFs stably expressing Ptch1-eGFP were incubated with Shh for 24 h in the presence or absence of 1 µM of purified GPC3-Ecto^{GAG+} or GPC3-Ecto^{GAG-}, and ciliary intensity of Ptch1 was measured by immunofluorescence microscopy. Cilia were detected by staining for endogenous Arl13B. GPC3-Ecto^{GAG+} and GPC3-Ecto^{GAG-} had no effect on Shh-induced Ptch1 exit from cilia. Data are mean±s.d. (300-400 cilia were measured per condition). (C) As in B but treating wild-type MEFs with SAG (1 µM) and measuring the intensity of endogenous Smo in primary cilia. GPC3-Ecto^{GAG+} and GPC3-Ecto^{GAG-} had no effect on SAG-induced ciliary accumulation of Smo. Data are mean±s.d. (300-400 cilia were measured per condition). (D) As in C but measuring the intensity of endogenous Gli proteins in primary cilia. GPC3-Ecto^{GAG+} abolishes Gli recruitment to ciliary tips by Hh pathway activation, whereas GPC3-Ecto^{GAG-} has no effect. Data are mean±s.d. (300-400 cilia were measured per condition). (E) As in D but cells were analyzed by immunoblotting for Gli1 and Gli3. Blotting for tubulin served as a loading control. GPC3-Ecto^{GAG+} did not block the reduction in Gli3R levels caused by Hh pathway activation but blocks the accumulation of Gli1. Blots shown are representative of three experiments. *P<0.05; n.s., not significant (two-tailed paired t-test). AU, arbitrary units.

downstream of Smo, as observed for *Gpc3*^{KO} cells. Finally, GPC3-Ecto^{GAG+} had no effect on Gli3FL and Gli3R levels but inhibited signal-dependent Gli1 protein accumulation (Fig. 3E), as seen with *Gpc3*^{KO} cells. In summary, the parallel phenotypes of *Gpc3*^{KO} cells and wild-type cells treated with GPC3-Ecto^{GAG+} support the idea that the GAG-modified GPC3 ectodomain functions in a dominant-negative fashion to antagonize Hh signaling.

Activity of GPC3-Ecto^{GAG+} in the Hh pathway requires heparan but not chondroitin sulfate

We took advantage of the activity of exogenously added purified GPC3-Ecto to dissect the biochemical requirements for GPC3 function. Specifically, we used this system to test the role of specific GAG modifications, a question impossible to address unambiguously by genetic approaches in cell culture or whole organisms.

Journal of Cell Science (2022) 135, jcs259297. doi:10.1242/jcs.259297

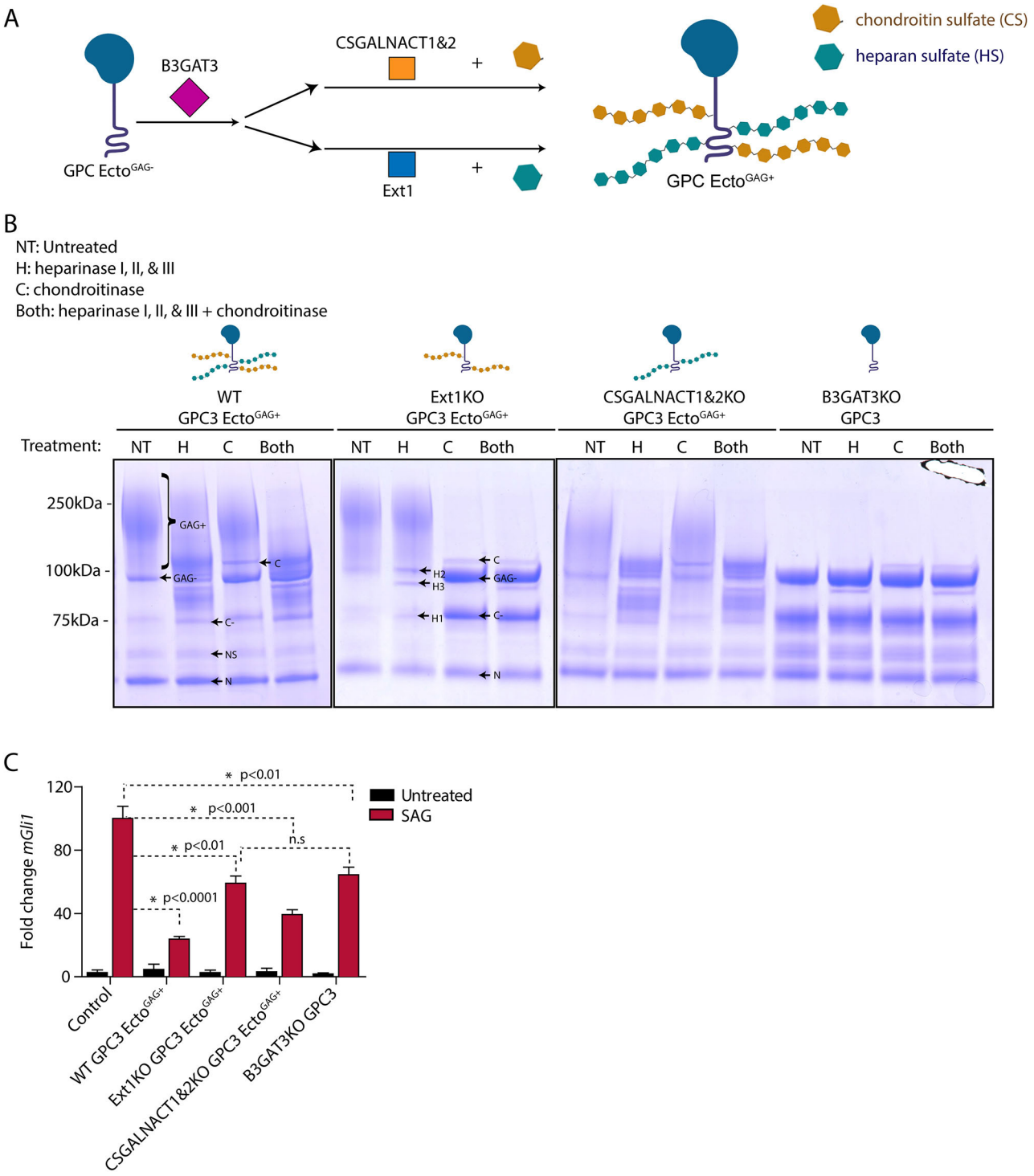

Fig. 4. Heparan sulfate modification is required for the effect of GPC3 on Hh signaling. (A) Schematic of the pathways for glypican modification with heparan sulfate (teal) or chondroitin sulfate (brown). B3GAT3 functions in the synthesis of the tetrasaccharide linker shared between chondroitin sulfate and heparan sulfate. CSGALNACT1 and 2 function in CS biosynthesis, whereas EXT1 functions in HS biosynthesis. (B) GPC3-Ecto was expressed and purified from HEK293T cells of the indicated genetic backgrounds [wild-type (WT), *EXT1*^{KO}, *CSGALNACT1,2*^{KO}, or *B3GAT3*^{KO}]. The proteins were then digested with heparinase I, II and III (H), chondroitinase (C), or both, for 4 h at room temperature. The reactions were analyzed by SDS-PAGE and Coomassie staining. In wild-type cells, GPC3-Ecto was modified with both heparan sulfate and chondroitin sulfate chains. The choice of expression host cells allowed modification of GPC3-Ecto with heparan sulfate, chondroitin sulfate or both. GPC3-Ecto also underwent incomplete Furin-mediated proteolytic cleavage into two fragments (38 and 22 kDa; see Fig. S4F). Band notation is as follows: GAG+, GAG-modified full-length ectodomain and C-terminal cleavage product; GAG–, full-length ectodomain, uncleaved; N, N-terminal Furin cleavage product; C, chondroitinase; H1, heparinase I; H2, heparinase II; H3, heparinase III; C–, GAG– C-terminal Furin cleavage product; NS, nonspecific degradation product. See Fig. S4F for schematic. Gels shown are representative of three experiments. (C) Wild-type MEFs were incubated with SAG (1 µM) or control medium for 24 h in the absence or presence of the indicated differentially GAG-modified purified GPC3-Ecto (1 µM). Hh signaling was measured by qRT-PCR for *Gli1*. GPC3-Ecto required heparan sulfate chains to inhibit Hh signaling. Data are mean±s.e.m. of three replicates. **P*<0.05; n.s., not significant (two-tailed paired *t*-test).

Journal of Cell Science (2022) 135, jcs259297. doi:10.1242/jcs.259297

Heparan sulfate and chondroitin sulfate are two broad subfamilies of GAGs attached to proteoglycans (Kusche-Gullberg and Kjellen, 2003; Filmus et al., 2008; Prydz, 2015; Fig. 4A). Although most HSPGs and chondroitin sulfate proteoglycans (CSPGs) carry either heparan sulfate or chondroitin sulfate, others can carry both types of chains (Filmus et al., 2008; Prydz, 2015). Indeed, we observed that purified GPC3-Ecto preparations contained both heparan sulfate and chondroitin sulfate (Fig. 4B). To determine which class of GAG modification is required for GPC3 function in Hh signaling, we generated HEK293T cells lacking enzymes necessary for the attachment of heparan sulfate, chondroitin sulfate or both. Heparan sulfate chains were ablated by knocking out exostosin-1 (*EXT1*), a glycosyltransferase that catalyzes heparan sulfate elongation (McCormick et al., 2000; Presto et al., 2008). Chondroitin sulfate chains were ablated by knocking out chondroitin sulfate N-acetylgalactosaminyltransferase 1 and 2 (*CSGALNACT1* and *CSGALNACT2*), which are needed for chondroitin sulfate attachment. Heparan sulfate and chondroitin sulfate were removed together by knocking out beta-1,3-glucuronyltransferase 3 (*B3GAT3*), which is needed for the attachment of both GAGs to proteins (Fig. 4A; Kusche-Gullberg and Kjellen, 2003). We then stably expressed and purified GPC3-Ecto from these knockout cells (Fig. S4A-D). To confirm the identity of attached GAG chains, we treated purified GPC3-Ecto proteins with recombinant heparinase (I, II and III), chondroitinase or both, and assayed the protein by SDS-PAGE. We observed that GPC3-Ecto purified from wild-type cells, when treated with either heparinase or chondroitinase, retained high-molecular weight GAG-modified material (Fig. 4B); however, treatment with both enzymes removed all GAG modifications (Fig. 4B), suggesting that purified GPC3-Ecto contains both heparan sulfate and chondroitin sulfate. As expected, GAG modification of GPC3-Ecto secreted from *EXT1*^{KO} cells was removed by chondroitinase, whereas GAG modification of GPC3-Ecto secreted from *CSGALNACT1,2*^{KO} cells was removed by heparinase (Fig. 4B). Finally, GPC3-Ecto secreted from *B3GAT3*^{KO} cells contained only unmodified core protein (Fig. 4B). Thus, purified GPC3-Ecto is typically modified with a mix of heparan sulfate and chondroitin sulfate but selectively bears either modification when isolated from cells defective for the other branch of GAG biosynthesis.

We used the GPC3-Ecto variants purified above to dissect the role of heparan sulfate and chondroitin sulfate modification. We found that GPC3-Ecto^{GAG+} from *CSGALNACT1,2*^{KO} cells (i.e. heparan sulfate modified) inhibited Hh pathway activation to a similar level as GPC3-Ecto^{GAG+} from wild-type cells (Fig. 4C), whereas GPC3-Ecto^{GAG+} from *EXT1*^{KO} cells (i.e. chondroitin sulfate modified) or GPC3-Ecto from *B3GAT3*^{KO} cells (i.e. unmodified) had a weaker effect than GPC3-Ecto from wild-type or *CSGALNACT1,2*^{KO} cells. As there was no significant difference between GPC3-Ecto from *EXT1*^{KO} cells and *B3GAT3*^{KO} cells, it would appear that heparan sulfate modification is the key contributing modification that causes Hh pathway inhibition. Similar results were obtained for the effect of GPC3-Ecto on constitutive Hh signaling in *Ptch1*$^{-/-}$ cells (Fig. S3A). Chondroitin sulfate-modified, heparan sulfate-modified and unmodified GPC3-Ecto had no effect on Wnt signaling (Fig. S4E), which is again consistent with the specific role of GPC3 towards the Hh pathway. Together, these data suggest that heparan sulfate modification is necessary for the effect of GPC3-Ecto on Hh signaling.

The GAG-modified unstructured stalk of GPC3 is necessary and sufficient for Hh pathway antagonism

Finally, we investigated which part of GPC3-Ecto is responsible for its activity on Hh signaling. All GPCs contain a large globular core domain and a flexible GAG-modified stalk (Kusche-Gullberg and Kjellen, 2003; Filmus et al., 2008; Prydz, 2015). To assay each portion of GPC3 separately, we purified a version of GPC3-Ecto carrying N- and C-terminal affinity tags, and a PreScission protease site between the globular core and the stalk (GPC3-Ecto^{PreScission}; Fig. 5A). This fusion protein was cleaved with PreScission, and the resulting core and stalk fragments were affinity purified (Fig. 5B) and tested separately in signaling assays. We found that the GAG-modified stalk protein potently inhibited Hh signaling in both wild-type (Fig. 5C) and *Ptch1*$^{-/-}$ cells (Fig. S3A), and the globular core had a slight but not statistically significant effect on signaling (Fig. 5C). Importantly, unmodified stalk purified from *B3GAT3*^{KO} cells was inactive (Fig. 5D) compared to the GAG-modified GPC3 stalk. These results indicate that the GPC3 stalk region, with its associated heparan sulfate, is necessary and sufficient for activity.

The experiments above cannot rule out that the GPC3 globular core might direct GAG modification of the stalk during biosynthesis. To investigate this possibility, we performed domain swaps between GPC3 and GPC1 or GPC2 (Fig. 5E), two GPCs that have no effect on Hh signaling when added as purified ectodomains (Fig. 5F). We found that purified chimeras containing the GPC3 stalk (GPC1^{core}-GPC3stalk-Ecto and GPC2^{core}-GPC3stalk-Ecto) inhibited Hh signaling but the reciprocal chimeras were inactive (Fig. 5F). Together, these results demonstrate that the stalk region of GPC3 is necessary and sufficient for directing its own heparan sulfate modification, which is required for its effect on Hh signaling.

DISCUSSION

GPCs have long been implicated in cell-cell signaling and tissue homeostasis, yet their mechanisms remain obscure. In this study, we investigated the role of GPC3 in Hh signaling. We found that cells lacking GPC3 exhibit greatly reduced Hh pathway activation, and that the soluble GPC3 ectodomain acts in dominant-negative fashion, phenocopying the effect of GPC3 loss on Hh signaling (Fig. 6B). Interestingly, recruiting the GPC3 ectodomain to the cell surface rescues the full Hh response, indicating that membrane attachment is critical for the role of GPC3 in promoting Hh signaling (Fig. 6A). Surprisingly, epistatic analysis indicated that the upstream steps in Hh pathway activation are unaffected by GPC3, as both Shh-mediated inhibition of Ptch1 and subsequent Smo activation occurred normally. In contrast, activation of downstream Gli proteins was severely affected by GPC3 inhibition, as evidenced by the defective recruitment of full-length Gli to cilia in response to Smo activation and by the reduced Gli-driven transcriptional output of the Hh pathway. Together, these results define a novel glypican-dependent pathway that modulates the strength of Hh signaling in responding cells.

Our results differ from previous studies of GPCs, which reported both positive (Li et al., 2011; Wilson and Stoeckli, 2013; Capurro et al., 2017) and negative (Capurro et al., 2008) roles in Hh signaling. To our knowledge, all these previous studies posited that GPCs act at the level of Shh reception by responding cells. In studies showing a positive role of GPCs in Hh signaling, GPCs were proposed to enhance Shh recruitment to cells (Witt et al., 2013), or Shh binding to Ptch1 (Li et al., 2011; Wilson and Stoeckli, 2013; Capurro et al., 2017). In instances of Hh antagonism, GPCs were proposed to compete with Ptch1 for binding to Shh (Capurro et al., 2008). We did not detect GPC3 binding to Shh, or an effect of GPC3 on the Shh-Ptch1 interaction. Moreover, we found that GPC3 inhibition affects not only Hh pathway activation by Shh but also downstream activation, at the level of Smo. Finally, we observed a specific defect in the ciliary recruitment of Gli proteins, and Ptch1

Journal of Cell Science (2022) 135, jcs259297. doi:10.1242/jcs.259297

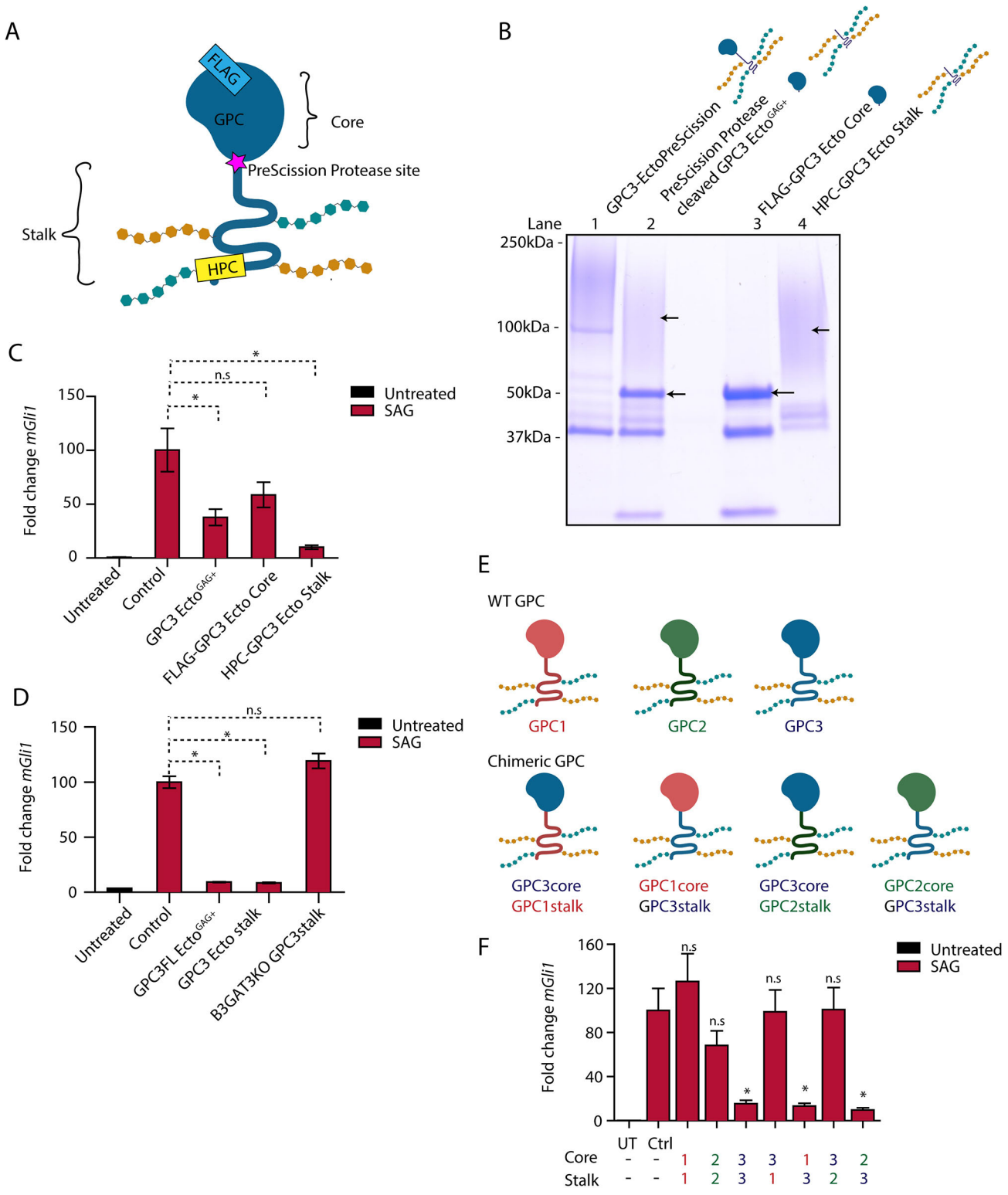

Fig. 5. See next page for legend.

and Smo ciliary dynamics were unaffected by GPC3 inhibition. Together, our results suggest that GPC3 is required for Hh signaling at a step subsequent to Smo activation, likely at the level of coupling between active Smo and Gli proteins.

GPC3 is mutated in Simpson–Golabi–Behmel syndrome, with 75% of GPC3 lesions being large deletions, frameshifts and truncating nonsense mutations; most of these mutations likely cause GPC3 loss or misfolding (Vuillaume et al., 2018). Interestingly, among the few characterized GPC3 missense mutations, one occurs in the sequence encoding the GPI anchor, resulting in the production of heparan sulfate-modified GPC3 ectodomain (Vuillaume et al., 2018); this disease mutant is consistent with the dominant-negative effect that we observed with purified GPC3-Ecto^{GAG+}.

Journal of Cell Science (2022) 135, jcs259297. doi:10.1242/jcs.259297

Fig. 5. The GAG-modified GPC3 stalk is necessary and sufficient for Hh pathway antagonism. (A) Schematic of the GPC3-Ecto variant with an engineered PreScission protease cleavage site between the core and stalk domains (GPC3-Ecto^{PreScission}). The fusion is FLAG tagged on the N terminus (to isolate the core domain after cleavage, FLAG-GPC3core) and HPC tagged on the C terminus (to isolate the stalk region, HPC-GPC3 stalk). (B) Affinity-purified GPC3-Ecto^{PreScission} (lane 1) was cleaved with PreScission protease (lane 2), followed by purification of the core domain (lane 3) and stalk (lane 4) by FLAG and HPC affinity, respectively. Proteins were analyzed by SDS-PAGE and Coomassie staining. Following protease cleavage, the globular core collapsed to defined bands (lane 3), whereas the stalk region migrated as a high molecular weight smear (lane 4) due to GAG modification. Gel shown is representative of three experiments. (C) Wild-type (WT) MEFs were incubated with SAG (1 µM) in the absence or presence of the indicated purified proteins (1 µM) for 24 h. Hh signaling was measured by qRT-PCR for *Gli1*. The GAG-modified GPC3 stalk potently inhibited Hh signaling, in contrast to the unmodified globular core. Untreated is no treatment. Cells were kept in DMEM. (D) As in C but with incubation with GPC3 stalk expressed and purified from *B3GAT3*^{KO} cells. The unmodified GPC3 stalk did not inhibit Hh signaling. (E) Schematic of GPCs GPC1, GPC2 and GPC3, and the chimeric GPCs generated by domain swapping. (F) As in C but with incubation with purified chimeric GPC ectodomains. Hh signaling antagonism required the presence of the GPC3 stalk.; Ctrl, cells treated with the buffer for the purified protein; UT, untreated. Data are mean±s.e.m. of three replicates. **P*<0.05; n.s., not significant (two-tailed paired *t*-test).

How might GPC3 regulate the Hh pathway? Although the molecular events that connect GPC3 to Gli protein activation remain to be elucidated, our results permit some speculation on the mechanism of GPC3. Previous work identified GPR161 as a repressor of Hh signaling epistatic to Smo, acting at the level of Gli3R. In the absence of GPR161, Gli3R is completely lost (Mukhopadhyay et al., 2013); in contrast, GPC3 inhibition did not change in Gli3R levels, suggesting that GPC3 might not be involved in the GPR161 branch of the Hh pathway. The phenotype of GPC3 inhibition, characterized by normal Smo entry into cilia but loss of Gli recruitment, resembles that caused by the loss of the KIF7 kinesin (Endoh-Yamagami et al., 2009; He et al., 2014) or one of its upstream regulators, such as DLG5 (Chong et al., 2015) or PPFI1A/PP2A (Liu et al., 2014). One possibility is that GPC3 acts in a signal transduction process upstream of one of these factors; for example, to control KIF7 phosphorylation and thus the regulation of Gli proteins in cilia. Finally, another possibility is that GPC3 might function as a scaffold that brings together other factors on the cell surface to promote a signaling event that impacts Gli recruitment to cilia; such a scaffolding role would explain the inhibitory effect of abnormally high expression of full-length GPC3, or the dominant-negative effect of purified GPC3 ectodomain.

Our results indicate that GPC3 is acutely required for Hh pathway activation. Recruitment of GPC3 ectodomain to the surface of *Gpc3*^{KO} cells rescues Gli recruitment to cilia tips in less than 6 h. Thus, changes in GPC3 function are translated over a relatively short timescale into corresponding changes in Hh pathway activation, possibly suggesting a transcription-independent mechanism for downstream Hh pathway modulation by GPC3.

Our functional analysis of purified GPC3 constructs afforded several mechanistic insights. First, GPC3 activity depends critically on its modification with GAG chains. Though purified GPC3-Ecto is modified with both heparan sulfate and chondroitin sulfate, we found, using protein purified from cells lacking one or both GAG biosynthetic pathways, that only the heparan sulfate-modified protein is active in Hh signaling. Deletion analysis surprisingly revealed that the GPC3 stalk region is necessary and sufficient for directing its own modification with heparan sulfate, and for its effect on Hh signaling. Although we observed that the GPC3 globular core is dispensable for the dominant-negative effect on the Hh pathway, we cannot rule out the possibility that putative endogenous binding partners might interact not only with stalk-associated heparan sulfate chains but also with the GPC3 core. Interestingly, we found that, in contrast to GPC3-Ecto, the ectodomains belonging to GPCs GPC1 and GPC2 are inactive in Hh signaling. This observation suggests that the discrete molecular structure of glypican-associated heparan sulfate – including the position, pattern and extent of sulfation – may differ between glypican family members. Further characterization of GPC3-associated heparan sulfate, together with functional assays of GPC3 purified from cells deficient in finer-scale heparan sulfate substructure biosynthesis, will be required to define the precise molecular requirements for GPC3 function.

Previous studies of GPCs employed genetic and molecular approaches with limited ability to precisely manipulate the GAG structure of individual GPCs. The present approach, relying on separate systems for GPC biosynthesis and functional interrogation, provides a powerful and general framework for mechanistic dissection. The availability of comprehensive collections of GAG biosynthesis knockout cells (Chen et al., 2018) should greatly facilitate expression and purification of proteoglycans bearing precisely edited GAG chains. Additionally, the heterologous cell-surface recruitment assay we describe can serve as a general platform for biochemical complementation of proteoglycan loss of

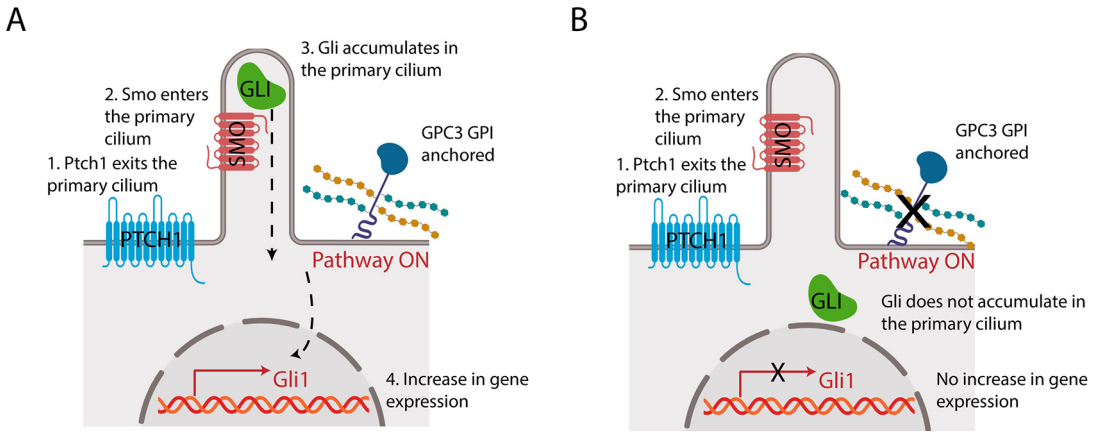

Fig. 6. Model of GPC3 function in Hh signaling. (A) Endogenous GPI-anchored GPC3 promotes Hh signaling at the level of Gli proteins. (B) Loss of GPC3 impairs Hh signaling.

Journal of Cell Science (2022) 135, jcs259297. doi:10.1242/jcs.259297

function. Together, these approaches should catalyze functional studies of proteoglycans with an unprecedented level of mechanistic detail, leading to important basic scientific and therapeutic insights.

MATERIALS AND METHODS

Cell lines

Human embryonic kidney cells (HEK293T; ATCC) and MEFs (gift from Dr Jim R. Woodgett, Lunenfeld-Tanenbaum Research Institute, Toronto, Canada) were grown in Dulbecco's modified Eagle's medium (DMEM), with 10% (v/v) fetal bovine serum (FBS) and penicillin/streptomycin. Stable cell lines were generated by infection with lentiviruses expressing genes of interest. Briefly, genes of interest were subcloned into the third-generation lentiviral vector pHAGE (Mostoslavsky et al., 2006), which was used to produce lentiviruses in HEK293T cells, as described previously (Wierbowski et al., 2020). Lentiviruses were mixed with 1 µg/ml hexadimethrine bromide (Sigma-Aldrich) and were used to infect the desired target cells. 48 h post-infection, stably transduced cells were isolated by selection with blasticidin (InvivoGen) or puromycin (InvivoGen).

CRISPR/Cas9 gene editing

Guide RNA (gRNA) sequences were designed to target murine *Gpc3*, human *EXT1*, human *CSGALNACT1*, human *CSGALNACT2* and human *B3GAT3* (http://chopchop.cbu.uib.no). Synthetic oligonucleotides (Integrated DNA Technologies) containing gRNA sequences were annealed and cloned into the pX459 vector (Ran et al., 2013). Parental cells were transfected with the gRNA-expressing plasmids, and were transiently selected with puromycin. The cells were then plated and grown clonally. Genomic DNA was extracted from individual clones, and the gRNA target loci were PCR amplified, followed by sequencing using an MiSeq instrument (Illumina). Characterization of CRISPR-induced genomic lesions of the null clones used in this study is shown in Table S1.

Antibodies and chemicals

Primary antibodies for immunoblotting were used at 1 µg/ml in blocking solution, consisting of TBST [10 mM Tris (pH 8), 150 mM NaCl and 0.2% Triton X-100] supplemented with 5% non-fat dry milk. Primary antibodies for immunoblots were as follows: goat anti-Gli1 (R&D Systems, AF3455; 1:500); goat anti-Gli3 (R&D Systems, AF3690; 1:500); and mouse monoclonal anti-tubulin (Sigma-Aldrich, T6199; DM1; 1:1000). Anti-goat IgG and anti-mouse IgG horseradish peroxidase-conjugated secondary antibodies (GE Healthcare) were used (1:5000 dilution) in blocking solution. For immunofluorescence, primary and secondary antibodies were used at 1 µg/ml in TBST supplemented with 5% bovine serum albumin. Primary antibodies for immunofluorescence were as follows: rabbit anti-GFP (1:1000) (Petrov et al., 2020); chicken anti-Arl13B (1:2000) (Petrov et al., 2020); rabbit anti-Gli2/3 (1:500) (Tukachinsky et al., 2016); and goat anti-Smo (1:1000) (Nedelcu et al., 2013). Fluorophore-conjugated secondary antibodies were as follows: donkey anti-chicken IgY-Alexa Fluor 647 (Jackson ImmunoResearch); donkey anti-goat IgG-Alexa Fluor 594 (Jackson ImmunoResearch); and donkey anti-rabbit IgG-Alexa Fluor 488 (Thermo Fisher). SAG (≥98%) was obtained from Axxora.

Hh and Wnt ligands

Shh-conditioned medium was produced as described previously (Nedelcu et al., 2013). Briefly, an expression construct encoding the first 197 amino acids of human Shh cloned in the pCS2 vector was transiently transfected into HEK293T cells, using polyethyleneimine. The next day, the medium was replaced with DMEM, and the cells were incubated for 48 h. The conditioned medium was collected, centrifuged to remove cellular debris and then used in signaling assays. Wnt3A-conditioned medium was produced using L cells stably expressing mouse Wnt3A (American Type Culture Collection). After reaching confluency, the cells were incubated in DMEM supplemented with 1% FBS for 48 h. The medium was harvested, centrifuged and used in Wnt signaling assays.

DNA constructs

Constructs were generated by PCR and were subcloned into the lentiviral pHAGE vector, driven by a human CMV promoter. The pHAGE constructs were used to produce lentiviruses for generating stable cell lines. The construct for expressing mouse Ptch1 tagged with eGFP at the C terminus has been described previously (Tukachinsky et al., 2016). Additional eGFP-tagged receptor constructs for cell-based ligand-receptor binding experiments, including Cdon, Boc and membrane-anchored single chain variable fragment 5E1 antibody (scFv5E1), have been described previously (Wierbowski et al., 2020). The genes used in this study were as follows: human GPC1 (NM_002081.3); human GPC2 (NM_152742.3); mouse GPC3 (NM_016697.3); human GPC4 (NM_001448.3); human GPC5 (NM_004466.6); human GPC6 (NM_005708.5); human SDC1 (NM_001006946.2); and human Hhip (NM_022475.3). The Hhip expression construct consisted of the human calreticulin signal sequence, one copy of eGFP and a flexible $(GGGSGGGT)_3$ linker, followed by the entire Hhip sequence after the portion encoding the N-terminal signal sequence. Full-length GPC expression constructs consisted of the influenza hemagglutinin signal sequence, one copy of eGFP or the FLAG or human protein C (HPC) epitope, followed by the GPC sequence after the portion encoding the N-terminal signal sequence. Constructs for expressing secreted fusion proteins (comprising entire GPC ectodomains or portions thereof) consisted of the following: signal sequence (endogenous or from influenza hemagglutinin), the GPC fragment, a flexible $(GGGSGGGT)_3$ linker, the mutant bacterial dehalogenase HaloTag7 (Ohana et al., 2009) and one copy of the HPC epitope. Some constructs also included PreScission protease cleavage sites for tag removal. Details of the new expression plasmids used in this study are provided in Table S2.

SDS-PAGE and immunoblotting

Protein samples were separated by SDS-PAGE on 4-20% gradient gels (Mini-PROTEAN TGX, Bio-Rad). Gels were soaked in transfer buffer [48 mM Tris (pH 9.2), 39 mM glycine, 1.3 mM SDS and 20% methanol], and were blotted by semi-dry transfer (Trans-Blot SD, Bio-Rad) onto nitrocellulose membranes (Millipore). For immunoblotting, the membranes were incubated for 30 min in blocking solution, followed by overnight incubation at 4°C with primary antibodies. Following three washes with TBST at room temperature, the membranes were incubated with secondary antibodies in blocking solution for 1 h at room temperature. The membranes were then washed three times with TBST and twice with TBS [10 mM Tris (pH 8) and 150 mM NaCl], followed by chemiluminescent detection (ECL, PerkinElmer).

Immunofluorescence microscopy

MEFs were plated on 12-mm diameter gelatin-coated round glass coverslips, in 24-well plates, at a density of 10^5 cells per well. Following overnight incubation, the complete medium was replaced with serum-free DMEM to induce ciliogenesis. After 24 h, the cells were treated with the indicated factors in serum-free DMEM for another 24 h. The cells were then fixed in PBS with 3.7% formaldehyde for 30 min at room temperature. Following permeabilization with TBST, endogenous Smo, endogenous Gli2/3 or overexpressed Ptch1-eGFP was detected by immunofluorescence microscopy. Cells were co-stained for endogenous Arl13B to detect primary cilia. The stained coverslips were mounted in PBS with 50% glycerol and were imaged using a Nikon TE2000E wide-field epifluorescence microscope equipped with an OrcaER camera (Hamamatsu) and a 40× PlanApo 0.45NA air objective (Nikon), as described previously (Nedelcu et al., 2013). For each condition, MetaMorph software (Molecular Devices) was used to acquire *z*-series consisting of five focal planes for at least 30 fields of view for fluorescence channels corresponding to Arl13B, and Smo, Gli2/3 or GFP. The *z*-series were used to generate maximum intensity projections, which were analyzed using custom image analysis scripts written in MATLAB (MathWorks). Briefly, cilia were segmented by local adaptive thresholding of Arl13B images and, for each cilium, background-corrected fluorescence intensity for Smo, Gli2/3 or eGFP fluorescence intensity was calculated. Data are presented as mean±s.e.m. across three biological replicates. $P<0.05$ was considered significant.

Fluorescent Shh ligands

Alexa Fluor594-labeled unlipidated Shh was produced as described previously (Petrov et al., 2021). Briefly, mouse Shh N-terminal signaling

domain (amino acids 24-198) was expressed in bacteria as a glutathione S-transferase (GST) fusion and was purified on glutathione agarose (GE Healthcare). Following cleavage of the GST tag with thrombin, Shh was purified by chromatography on heparin agarose (GE Healthcare) using a linear NaCl elution gradient [0.15 M to 1 M NaCl, in 25 mM phosphate (pH 7.2)]. Purified Shh was supplemented with TCEP (10 mM, pH 7.5) and incubated for 3 h at room temperature with a threefold molar excess of Alexa Fluor 594-maleimide (Thermo Fisher Scientific) to label the N-terminal cysteine. Unreacted Alexa Fluor 594-maleimide was removed on a NAP-10 desalting column (GE Healthcare). Tetramethylrhodamine (TMR)-labeled palmitoylated Shh was produced as described previously (Wierbowski et al., 2020). Briefly, human Shh N-terminal signaling domain (amino acids 24-197), tagged C-terminally with HaloTag7 and HPC epitope, was expressed in mammalian cells and purified via anti-HPC affinity chromatography from conditioned medium. The protein was then incubated for 1 h at room temperature with a fivefold molar excess of HaloTag TMR ligand (Promega), followed by removal of the unreacted dye on a NAP-5 desalting column (GE Healthcare).

Cell-based Shh binding assays

HEK293T cells plated in poly-D-lysine-coated wells were transfected with the eGFP-tagged receptor constructs and were grown for 48 h. The cells were incubated in OptiMEM with Alexa Fluor594-labeled unlipidated Shh or TMR-labeled palmitoylated Shh for 1.5 h at 37°C. For competition experiments, the fluorescent Shh ligand and the competitor [purified unlipidated Shh, scFv5E1 anti-Shh single-chain antibody (Wierbowski et al., 2020) or GPC3-Ecto] were pre-incubated before addition to cells for 30 min at room temperature. After incubation, the cells were washed with OptiMEM and were fixed in PBS with 3.7% formaldehyde for 30 min at room temperature. Fixed cells were washed twice with PBS and imaged by fluorescence microscopy using a 10× PlanApo 0.45NA objective (Nikon). For each condition, ligand and receptor images were acquired for four fields of view (MetaMorph software, Molecular Devices). Images were analyzed as described previously (Wierbowski et al., 2020). Briefly, cells were segmented based on the eGFP signal, and the background-subtracted fluorescence intensity of the Shh ligand was calculated. Bound ligand is measured as the ratio of total Shh intensity to area for each segmented cell, and is represented as a boxplot spanning from the first to the third quartile of the distribution. For statistical testing, the median bound ligand was calculated for three random non-overlapping subsets of the cell population measured for each condition. Ordinary one-way ANOVA, with Dunnett's multiple comparisons test, was performed on the sets of three medians to calculate *P*-values, using the first condition (Smo in Fig. 1C,D, and control competitor for Fig. 1E) as the reference sample.

qRT-PCR

MEF lines were plated in triplicate in six-well plates and, after reaching confluency, were serum starved overnight. Afterwards, the cells were treated with the indicated factors in DMEM for 24 h. Total RNA was isolated using TRIzol (Thermo Fisher Scientific), after which the RNA was treated with DNase I (Promega), followed by a second round of TRIzol purification. The RNA was reverse transcribed using Luna SuperScript (New England Biolabs) and random hexamers. To measure Hh pathway activation, the target gene *Gli1* and the control gene *cyclophilin* were measured with Power SYBR Green (Thermo Fisher Scientific), as described previously (Liu et al., 2014). The primer sequences are listed in Table S3. Control cells were treated with storage buffer [20 mM Na-HEPES (pH 7.5) and 200 mM NaCl] that was used to preserve the purified proteins. The comparative Ct method (Schmittgen and Livak, 2008) was used to compute the expression of *Gli1* relative to *cyclophilin*. Data for Hh pathway activation was normalized from 0% (untreated) to 100% (saturating amounts of the Smo agonist SAG). Data are presented as mean±s.e.m. across three biological replicates. $P<0.05$ was considered significant.

Protein expression and purification

Secreted proteins (GPC ectodomains and fragments thereof, and scFv5E1) were stably expressed in HEK293T cells and affinity purified from conditioned medium using their C-terminal HPC tags. Briefly, cell lines producing the desired protein fusion were grown in DMEM with 10% FBS, in 10-20 15-cm plates, until they reached confluency. The medium was then changed to DMEM with 1% FBS, and three collections were performed, each over 48 h. Conditioned medium was supplemented with $CaCl_2$ to 2 mM and centrifuged (5000 ***g***) and filtered (0.22 µm) to remove debris. The conditioned medium was loaded onto an anti-HPC affinity column, followed by extensive washing with TBS with 2 mM $CaCl_2$. Bound protein was eluted in elution buffer [20 mM Na-HEPES (pH 7.5), 200 mM NaCl, 5 mM EDTA and 100 µg/ml HPC peptide]. Eluted protein was concentrated using centrifugal filter units (10-kDa cutoff, Millipore) and further purified by size-exclusion chromatography (Superdex 200 10/300 GL column, GE Healthcare). Appropriate fractions were collected, pooled, concentrated using centrifugal filter units, flash-frozen and stored at −80°C until use.

Genes encoding heparinases I, II and III (*bt4675*, *bt4652* and *bt4657*) (Cartmell et al., 2017), and chondroitinase (*bt3350*), were cloned from *Bacteroides thetaiotaomicron* genomic DNA. Sequences encoding the enzymes lacking signal peptides were subcloned into the pGEX bacterial expression vector (GE Healthcare). GST-tagged proteins were expressed in BL21 DE3 pLysS *Escherichia coli* cells (Novagen) and purified as soluble proteins, according to the manufacturer's instructions. The activity and specificity of GST-tagged recombinant enzymes were confirmed by performing enzyme kinetic assays (measuring A232 absorbance) on porcine intestinal heparin (Sigma-Aldrich) or chondroitin sulfate A (Sigma-Aldrich) substrates. Purified proteins and activity assays are shown in Fig. S5, with specific activity measurements reported in Table S4.

Acknowledgements

We thank the Initiative for Gene Editing and Neurodegeneration (Cell Biology, Harvard Medical School) for help with MiSeq experiments; the Harvard Institute for Chemistry and Cell Biology for access to a QuantStudio 7 real-time PCR system; Pengxiang Huang for help with protein purification; Lina Yao (Devlin lab, Harvard Medical School) for the gift of *B. thetaiotaomicron* genomic DNA; and Marco Catipovic for critical reading of the manuscript.

Competing interests

The authors declare no competing or financial interests.

Author contributions

Conceptualization: Y.C.L., B.M.W., A.S.; Methodology: Y.C.L., B.M.W., A.S.; Software: Y.C.L., B.M.W.; Validation: Y.C.L., B.M.W., A.S.; Formal analysis: Y.C.L., B.M.W.; Investigation: Y.C.L., B.M.W., A.S.; Resources: Y.C.L., B.M.W., A.S.; Data curation: Y.C.L., B.M.W., A.S.; Writing - original draft: Y.C.L., B.M.W., A.S.; Writing - review & editing: Y.C.L., B.M.W., A.S.; Visualization: Y.C.L., B.M.W., A.S.; Supervision: A.S.; Project administration: Y.C.L., B.M.W., A.S.; Funding acquisition: Y.C.L., B.M.W., A.S.

Funding

This work was supported by the National Institutes of Health (R01 GM122920 and GM135262 to A.S; T32GM007226 and F31GM120833 to B.M.W.). Y.C.L. was supported by a Kidney Foundation of Canada KRESCENT postdoctoral fellowship. Deposited in PMC for release after 12 months.

Peer review history

The peer review history is available online at https://journals.biologists.com/jcs/article-lookup/doi/10.1242/jcs.259297.

References

Ahn, J., Lüdecke, H.-J., Lindow, S., Horton, W. A., Lee, B., Wagner, M. J., Horsthemke, B. and Wells, D. E. (1995). Cloning of the putative tumour suppressor gene for hereditary multiple exostoses (EXT1). *Nat. Genet.* **11**, 137-143. doi:10.1038/ng1095-137

Aza-Blanc, P., Lin, H. Y., Ruiz i Altaba, A. and Kornberg, T. B. (2000). Expression of the vertebrate Gli proteins in Drosophila reveals a distribution of activator and repressor activities. *Development* **127**, 4293-4301. doi:10.1242/dev.127.19.4293

Baeg, G. H., Lin, X., Khare, N., Baumgartner, S. and Perrimon, N. (2001). Heparan sulfate proteoglycans are critical for the organization of the extracellular distribution of Wingless. *Development* **128**, 87-94. doi:10.1242/dev.128.1.87

Bai, C. B. and Joyner, A. L. (2001). Gli1 can rescue the in vivo function of Gli2. *Development* **128**, 5161-5172. doi:10.1242/dev.128.24.5161

Bangs, F. and Anderson, K. V. (2017). Primary cilia and mammalian Hedgehog signaling. *Cold Spring Harb. Perspect. Biol.* **9**, a028175. doi:10.1101/cshperspect.a028175

Belenkaya, T. Y., Han, C., Yan, D., Opoka, R. J., Khodoun, M., Liu, H. and Lin, X. (2004). Drosophila Dpp morphogen movement is independent of dynamin-mediated endocytosis but regulated by the glypican members of heparan sulfate proteoglycans. *Cell* **119**, 231-244. doi:10.1016/j.cell.2004.09.031

Bellaiche, Y., The, I. and Perrimon, N. (1998). Tout-velu is a Drosophila homologue of the putative tumour suppressor EXT-1 and is needed for Hh diffusion. *Nature* **394**, 85-88. doi:10.1038/27932

Binari, R. C., Staveley, B. E., Johnson, W. A., Godavarti, R., Sasisekharan, R. and Manoukian, A. S. (1997). Genetic evidence that heparin-like glycosaminoglycans are involved in wingless signaling. *Development* **124**, 2623-2632. doi:10.1242/dev.124.13.2623

Bourdon, M. A., Krusius, T., Campbell, S., Schwartz, N. B. and Ruoslahti, E. (1987). Identification and synthesis of a recognition signal for the attachment of glycosaminoglycans to proteins. *Proc. Natl. Acad. Sci. USA* **84**, 3194-3198. doi:10.1073/pnas.84.10.3194

Bülow, H. E. and Hobert, O. (2006). The molecular diversity of glycosaminoglycans shapes animal development. *Annu. Rev. Cell Dev. Biol.* **22**, 375-407. doi:10.1146/annurev.cellbio.22.010605.093433

Campos-Xavier, A. B., Martinet, D., Bateman, J., Belluoccio, D., Rowley, L., Tan, T. Y., Baxová, A., Gustavson, K.-H., Borochowitz, Z. U., Innes, A. M. et al. (2009). Mutations in the heparan-sulfate proteoglycan glypican 6 (GPC6) impair endochondral ossification and cause recessive omodysplasia. *Am. J. Hum. Genet.* **84**, 760-770. doi:10.1016/j.ajhg.2009.05.002

Cano-Gauci, D. F., Song, H. H., Yang, H., McKerlie, C., Choo, B., Shi, W., Pullano, R., Piscione, T. D., Grisaru, S., Soon, S. et al. (1999). Glypican-3-deficient mice exhibit developmental overgrowth and some of the abnormalities typical of Simpson-Golabi-Behmel syndrome. *J. Cell Biol.* **146**, 255-264. doi:10.1083/jcb.146.1.255

Capurro, M. I., Xiang, Y.-Y., Lobe, C. and Filmus, J. (2005). Glypican-3 promotes the growth of hepatocellular carcinoma by stimulating canonical Wnt signaling. *Cancer Res.* **65**, 6245-6254. doi:10.1158/0008-5472.CAN-04-4244

Capurro, M. I., Xu, P., Shi, W., Li, F., Jia, A. and Filmus, J. (2008). Glypican-3 inhibits Hedgehog signaling during development by competing with patched for Hedgehog binding. *Dev. Cell* **14**, 700-711. doi:10.1016/j.devcel.2008.03.006

Capurro, M., Shi, W., Izumikawa, T., Kitagawa, H. and Filmus, J. (2015). Processing by convertases is required for glypican-3-induced inhibition of Hedgehog signaling. *J. Biol. Chem.* **290**, 7576-7585. doi:10.1074/jbc.M114.612705

Capurro, M., Izumikawa, T., Suarez, P., Shi, W., Cydzik, M., Kaneiwa, T., Gariepy, J., Bonafe, L. and Filmus, J. (2017). Glypican-6 promotes the growth of developing long bones by stimulating Hedgehog signaling. *J. Cell Biol.* **216**, 2911-2926. doi:10.1083/jcb.201605119

Cartmell, A., Lowe, E. C., Baslé, A., Firbank, S. J., Ndeh, D. A., Murray, H., Terrapon, N., Lombard, V., Henrissat, B., Turnbull, J. E. et al. (2017). How members of the human gut microbiota overcome the sulfation problem posed by glycosaminoglycans. *Proc. Natl. Acad. Sci. USA* **114**, 7037-7042. doi:10.1073/pnas.1704367114

Chen, J. K., Taipale, J., Young, K. E., Maiti, T. and Beachy, P. A. (2002). Small molecule modulation of Smoothened activity. *Proc. Natl. Acad. Sci. USA* **99**, 14071-14076. doi:10.1073/pnas.182542899

Chen, Y.-H., Narimatsu, Y., Clausen, T. M., Gomes, C., Karlsson, R., Steentoft, C., Spliid, C. B., Gustavsson, T., Salanti, A., Persson, A. et al. (2018). The GAGOme: a cell-based library of displayed glycosaminoglycans. *Nat. Methods* **15**, 881-888. doi:10.1038/s41592-018-0086-z

Chiao, E., Fisher, P., Crisponi, L., Deiana, M., Dragatsis, I., Schlessinger, D., Pilia, G. and Efstratiadis, A. (2002). Overgrowth of a mouse model of the Simpson-Golabi-Behmel syndrome is independent of IGF signaling. *Dev. Biol.* **243**, 185-206. doi:10.1006/dbio.2001.0554

Chong, Y. C., Mann, R. K., Zhao, C., Kato, M. and Beachy, P. A. (2015). Bifurcating action of Smoothened in Hedgehog signaling is mediated by Dlg5. *Genes Dev.* **29**, 262-276. doi:10.1101/gad.252676.114

Dahmane, N., Lee, J., Robins, P., Heller, P. and Ruiz i Altaba, A. (1997). Activation of the transcription factor Gli1 and the Sonic hedgehog signalling pathway in skin tumours. *Nature* **389**, 876-881. doi:10.1038/39918

David, G., Lories, V., Decock, B., Marynen, P., Cassiman, J. J. and Van den Berghe, H. (1990). Molecular cloning of a phosphatidylinositol-anchored membrane heparan sulfate proteoglycan from human lung fibroblasts. *J. Cell Biol.* **111**, 3165-3176. doi:10.1083/jcb.111.6.3165

de Boeck, H., Lories, V., David, G., Cassiman, J. J. and van den Berghe, H. (1987). Identification of a 64 kDa heparan sulphate proteoglycan core protein from human lung fibroblast plasma membranes with a monoclonal antibody. *Biochem. J.* **247**, 765-771. doi:10.1042/bj2470765

De Cat, B., Muyldermans, S.-Y., Coomans, C., Degeest, G., Vanderschueren, B., Creemers, J., Biemar, F., Peers, B. and David, G. (2003). Processing by proprotein convertases is required for glypican-3 modulation of cell survival, Wnt signaling, and gastrulation movements. *J. Cell Biol.* **163**, 625-635. doi:10.1083/jcb.200302152

Desbordes, S. C. and Sanson, B. (2003). The glypican Dally-like is required for Hedgehog signalling in the embryonic epidermis of Drosophila. *Development* **130**, 6245-6255. doi:10.1242/dev.00874

Dubey, R., van Kerkhof, P., Jordens, I., Malinauskas, T., Pusapati, G. V., McKenna, J. K., Li, D., Carette, J. E., Ho, M., Siebold, C. et al. (2020). R-spondins engage heparan sulfate proteoglycans to potentiate WNT signaling. *eLife* **9**, e54469. doi:10.7554/eLife.54469

Endoh-Yamagami, S., Evangelista, M., Wilson, D., Wen, X., Theunissen, J.-W., Phamluong, K., Davis, M., Scales, S. J., Solloway, M. J., de Sauvage, F. J. et al. (2009). The mammalian Cos2 homolog Kif7 plays an essential role in modulating Hh signal transduction during development. *Curr. Biol.* **19**, 1320-1326. doi:10.1016/j.cub.2009.06.046

Esko, J. D., Stewart, T. E. and Taylor, W. H. (1985). Animal cell mutants defective in glycosaminoglycan biosynthesis. *Proc. Natl. Acad. Sci. USA* **82**, 3197-3201. doi:10.1073/pnas.82.10.3197

Filmus, J. and Capurro, M. (2014). The role of glypicans in Hedgehog signaling. *Matrix Biol.* **35**, 248-252. doi:10.1016/j.matbio.2013.12.007

Filmus, J., Capurro, M. and Rast, J. (2008). Glypicans. *Genome Biol.* **9**, 224. doi:10.1186/gb-2008-9-5-224

Franch-Marro, X., Marchand, O., Piddini, E., Ricardo, S., Alexandre, C. and Vincent, J.-P. (2005). Glypicans shunt the Wingless signal between local signalling and further transport. *Development* **132**, 659-666. doi:10.1242/dev.01639

Gotzke, H., Kilisch, M., Martinez-Carranza, M., Sograte-Idrissi, S., Rajavel, A., Schlichthaerle, T., Engels, N., Jungmann, R., Stenmark, P., Opazo, F. et al. (2019). The ALFA-tag is a highly versatile tool for nanobody-based bioscience applications. *Nat. Commun.* **10**, 4403. doi:10.1038/s41467-019-12301-7

Grisaru, S. and Rosenblum, N. D. (2001). Glypicans and the biology of renal malformations. *Pediatr. Nephrol.* **16**, 302-306. doi:10.1007/s004670000530

Häcker, U., Lin, X. and Perrimon, N. (1997). The Drosophila sugarless gene modulates Wingless signaling and encodes an enzyme involved in polysaccharide biosynthesis. *Development* **124**, 3565-3573. doi:10.1242/dev.124.18.3565

Häcker, U., Nybakken, K. and Perrimon, N. (2005). Heparan sulphate proteoglycans: the sweet side of development. *Nat. Rev. Mol. Cell Biol.* **6**, 530-541. doi:10.1038/nrm1681

Haerry, T. E., Heslip, T. R., Marsh, J. L. and O'Connor, M. B. (1997). Defects in glucuronate biosynthesis disrupt Wingless signaling in Drosophila. *Development* **124**, 3055-3064. doi:10.1242/dev.124.16.3055

Han, C., Belenkaya, T. Y., Khodoun, M., Tauchi, M., Lin, X. and Lin, X. (2004a). Distinct and collaborative roles of Drosophila EXT family proteins in morphogen signalling and gradient formation. *Development* **131**, 1563-1575. doi:10.1242/dev.01051

Han, C., Belenkaya, T. Y., Wang, B. and Lin, X. (2004b). Drosophila glypicans control the cell-to-cell movement of Hedgehog by a dynamin-independent process. *Development* **131**, 601-611. doi:10.1242/dev.00958

Han, C., Yan, D., Belenkaya, T. Y. and Lin, X. (2005). Drosophila glypicans Dally and Dally-like shape the extracellular Wingless morphogen gradient in the wing disc. *Development* **132**, 667-679. doi:10.1242/dev.01636

He, M., Subramanian, R., Bangs, F., Omelchenko, T., Liem, K. F., Jr, Kapoor, T. M. and Anderson, K. V. (2014). The kinesin-4 protein Kif7 regulates mammalian Hedgehog signalling by organizing the cilium tip compartment. *Nat. Cell Biol.* **16**, 663-672. doi:10.1038/ncb2988

Holtz, A. M., Griffiths, S. C., Davis, S. J., Bishop, B., Siebold, C. and Allen, B. L. (2015). Secreted HHIP1 interacts with heparan sulfate and regulates Hedgehog ligand localization and function. *J. Cell Biol.* **209**, 739-758. doi:10.1083/jcb.201411024

Jackson, S. M., Nakato, H., Sugiura, M., Jannuzi, A., Oakes, R., Kaluza, V., Golden, C. and Selleck, S. B. (1997). dally, a Drosophila glypican, controls cellular responses to the TGF-beta-related morphogen, Dpp. *Development* **124**, 4113-4120. doi:10.1242/dev.124.20.4113

Jen, Y.-H. L., Musacchio, M. and Lander, A. D. (2009). Glypican-1 controls brain size through regulation of fibroblast growth factor signaling in early neurogenesis. *Neural Dev.* **4**, 33. doi:10.1186/1749-8104-4-33

Khare, N. and Baumgartner, S. (2000). Dally-like protein, a new Drosophila glypican with expression overlapping with wingless. *Mech. Dev.* **99**, 199-202. doi:10.1016/S0925-4773(00)00502-5

Kim, J., Kato, M. and Beachy, P. A. (2009). Gli2 trafficking links Hedgehog-dependent activation of Smoothened in the primary cilium to transcriptional activation in the nucleus. *Proc. Natl. Acad. Sci. USA* **106**, 21666-21671. doi:10.1073/pnas.0912180106

Kim, M.-S., Saunders, A. M., Hamaoka, B. Y., Beachy, P. A. and Leahy, D. J. (2011). Structure of the protein core of the glypican Dally-like and localization of a region important for hedgehog signaling. *Proc. Natl. Acad. Sci. USA* **108**, 13112-13117. doi:10.1073/pnas.1109877108

Kolluri, A. and Ho, M. (2019). The role of Glypican-3 in regulating Wnt, YAP, and Hedgehog in liver cancer. *Front. Oncol.* **9**, 708. doi:10.3389/fonc.2019.00708

Kusche-Gullberg, M. and Kjellen, L. (2003). Sulfotransferases in glycosaminoglycan biosynthesis. *Curr. Opin. Struct. Biol.* **13**, 605-611. doi:10.1016/j.sbi.2003.08.002

LeClair, E. E., Mui, S. R., Huang, A., Topczewska, J. M. and Topczewski, J. (2009). Craniofacial skeletal defects of adult zebrafish Glypican 4 (knypek) mutants. *Dev. Dyn.* **238**, 2550-2563. doi:10.1002/dvdy.22086

Li, F., Shi, W., Capurro, M. and Filmus, J. (2011). Glypican-5 stimulates rhabdomyosarcoma cell proliferation by activating Hedgehog signaling. *J. Cell Biol.* **192**, 691-704. doi:10.1083/jcb.201008087

Lin, X. and Perrimon, N. (1999). Dally cooperates with Drosophila Frizzled 2 to transduce Wingless signalling. *Nature* **400**, 281-284. doi:10.1038/22343

Liu, Y. C., Couzens, A. L., Deshwar, A. R., McBroom-Cerajewski, L. D. B., Zhang, X., Puviindran, V., Scott, I. C., Gingras, A. C., Hui, C.-C. and Angers, S. (2014). The PPFIA1-PP2A protein complex promotes trafficking of Kif7 to the ciliary tip and Hedgehog signaling. *Sci. Signal.* **7**, ra117. doi:10.1126/scisignal.2005608

Lum, L., Yao, S., Mozer, B., Rovescalli, A., Von Kessler, D., Nirenberg, M. and Beachy, P. A. (2003). Identification of Hedgehog pathway components by RNAi in Drosophila cultured cells. *Science* **299**, 2039-2045. doi:10.1126/science.1081403

McCormick, C., Duncan, G., Goutsos, K. T. and Tufaro, F. (2000). The putative tumor suppressors EXT1 and EXT2 form a stable complex that accumulates in the Golgi apparatus and catalyzes the synthesis of heparan sulfate. *Proc. Natl. Acad. Sci. USA* **97**, 668-673. doi:10.1073/pnas.97.2.668

Mostoslavsky, G., Fabian, A. J., Rooney, S., Alt, F. W. and Mulligan, R. C. (2006). Complete correction of murine Artemis immunodeficiency by lentiviral vector-mediated gene transfer. *Proc. Natl. Acad. Sci. USA* **103**, 16406-16411. doi:10.1073/pnas.0608130103

Mukhopadhyay, S., Wen, X., Ratti, N., Loktev, A., Rangell, L., Scales, S. J. and Jackson, P. K. (2013). The ciliary G-protein-coupled receptor Gpr161 negatively regulates the Sonic hedgehog pathway via cAMP signaling. *Cell* **152**, 210-223. doi:10.1016/j.cell.2012.12.026

Nakato, H., Futch, T. A. and Selleck, S. B. (1995). The division abnormally delayed (dally) gene: a putative integral membrane proteoglycan required for cell division patterning during postembryonic development of the nervous system in Drosophila. *Development* **121**, 3687-3702. doi:10.1242/dev.121.11.3687

Nedelcu, D., Liu, J., Xu, Y., Jao, C. and Salic, A. (2013). Oxysterol binding to the extracellular domain of Smoothened in Hedgehog signaling. *Nat. Chem. Biol.* **9**, 557-564. doi:10.1038/nchembio.1290

Ohana, R. F., Encell, L. P., Zhao, K., Simpson, D., Slater, M. R., Urh, M. and Wood, K. V. (2009). HaloTag7: a genetically engineered tag that enhances bacterial expression of soluble proteins and improves protein purification. *Protein Expr. Purif.* **68**, 110-120. doi:10.1016/j.pep.2009.05.010

Okamoto, K., Tokunaga, K., Doi, K., Fujita, T., Suzuki, H., Katoh, T., Watanabe, T., Nishida, N., Mabuchi, A., Takahashi, A. et al. (2011). Common variation in GPC5 is associated with acquired nephrotic syndrome. *Nat. Genet.* **43**, 459-463. doi:10.1038/ng.792

Okamoto, K., Honda, K., Doi, K., Ishizu, T., Katagiri, D., Wada, T., Tomita, K., Ohtake, T., Kaneko, T., Kobayashi, S. et al. (2015). Glypican-5 increases susceptibility to nephrotic damage in diabetic kidney. *Am. J. Pathol.* **185**, 1889-1898. doi:10.1016/j.ajpath.2015.03.025

Pei, J. and Grishin, N. V. (2012). Cysteine-rich domains related to Frizzled receptors and Hedgehog-interacting proteins. *Protein Sci.* **21**, 1172-1184. doi:10.1002/pro.2105

Petrov, K., Wierbowski, B. M. and Salic, A. (2017). Sending and Receiving Hedgehog Signals. *Annu. Rev. Cell Dev. Biol.* **33**, 145-168. doi:10.1146/annurev-cellbio-100616-060847

Petrov, K., Wierbowski, B. M., Liu, J. and Salic, A. (2020). Distinct cation gradients power cholesterol transport at different key points in the Hedgehog signaling pathway. *Dev. Cell* **55**, 314-327.e17. doi:10.1016/j.devcel.2020.08.002

Petrov, K., de Almeida Magalhaes, T. and Salic, A. (2021). Mechanism and ultrasensitivity in Hedgehog signaling revealed by Patched1 disease mutations. *Proc. Natl Acad. Sci. USA* **118**, e2006800118. doi:10.1073/pnas.2006800118

Pilia, G., Hughes-Benzie, R. M., MacKenzie, A., Baybayan, P., Chen, E. Y., Huber, R., Neri, G., Cao, A., Forabosco, A. and Schlessinger, D. (1996). Mutations in GPC3, a glypican gene, cause the Simpson-Golabi-Behmel overgrowth syndrome. *Nat. Genet.* **12**, 241-247. doi:10.1038/ng0396-241

Prabhakar, V., Capila, I. and Sasisekharan, R. (2009). The structural elucidation of glycosaminoglycans. *Methods Mol. Biol.* **534**, 147-156. doi:10.1007/978-1-59745-022-5_11

Presto, J., Thuveson, M., Carlsson, P., Busse, M., Wilen, M., Eriksson, I., Kusche-Gullberg, M. and Kjellen, L. (2008). Heparan sulfate biosynthesis enzymes EXT1 and EXT2 affect NDST1 expression and heparan sulfate sulfation. *Proc. Natl. Acad. Sci. USA* **105**, 4751-4756. doi:10.1073/pnas.0705807105

Prydz, K. (2015). Determinants of Glycosaminoglycan (GAG) Structure. *Biomolecules* **5**, 2003-2022. doi:10.3390/biom5032003

Ran, F. A., Hsu, P. D., Wright, J., Agarwala, V., Scott, D. A. and Zhang, F. (2013). Genome engineering using the CRISPR-Cas9 system. *Nat. Protoc.* **8**, 2281-2308. doi:10.1038/nprot.2013.143

Roberts, I. S. D. and Gleadle, J. M. (2008). Familial nephropathy and multiple exostoses with exostosin-1 (EXT1) gene mutation. *J. Am. Soc. Nephrol.* **19**, 450-453. doi:10.1681/ASN.2007080842

Rohatgi, R., Milenkovic, L. and Scott, M. P. (2007). Patched1 regulates hedgehog signaling at the primary cilium. *Science* **317**, 372-376. doi:10.1126/science.1139740

Sarrazin, S., Lamanna, W. C. and Esko, J. D. (2011). Heparan sulfate proteoglycans. *Cold Spring Harb. Perspect. Biol.* **3**, a004952. doi:10.1101/cshperspect.a004952

Schmittgen, T. D. and Livak, K. J. (2008). Analyzing real-time PCR data by the comparative C(T) method. *Nat. Protoc.* **3**, 1101-1108. doi:10.1038/nprot.2008.73

Selleck, S. B. (1999). Overgrowth syndromes and the regulation of signaling complexes by proteoglycans. *Am. J. Hum. Genet.* **64**, 372-377. doi:10.1086/302266

Shi, W. and Filmus, J. (2009). A patient with the Simpson-Golabi-Behmel syndrome displays a loss-of-function point mutation in GPC3 that inhibits the attachment of this proteoglycan to the cell surface. *Am. J. Med. Genet. A* **149A**, 552-554. doi:10.1002/ajmg.a.32669

Song, H. H., Shi, W., Xiang, Y.-Y. and Filmus, J. (2005). The loss of glypican-3 induces alterations in Wnt signaling. *J. Biol. Chem.* **280**, 2116-2125. doi:10.1074/jbc.M410090200

Stipp, C. S., Litwack, E. D. and Lander, A. D. (1994). Cerebroglycan: an integral membrane heparan sulfate proteoglycan that is unique to the developing nervous system and expressed specifically during neuronal differentiation. *J. Cell Biol.* **124**, 149-160. doi:10.1083/jcb.124.1.149

Svensson, G., Awad, W., Håkansson, M., Mani, K. and Logan, D. T. (2012). Crystal structure of N-glycosylated human glypican-1 core protein: structure of two loops evolutionarily conserved in vertebrate glypican-1. *J. Biol. Chem.* **287**, 14040-14051. doi:10.1074/jbc.M111.322487

Takei, Y., Ozawa, Y., Sato, M., Watanabe, A. and Tabata, T. (2004). Three Drosophila EXT genes shape morphogen gradients through synthesis of heparan sulfate proteoglycans. *Development* **131**, 73-82. doi:10.1242/dev.00913

Teng, Y. H.-F., Aquino, R. S. and Park, P. W. (2012). Molecular functions of syndecan-1 in disease. *Matrix Biol.* **31**, 3-16. doi:10.1016/j.matbio.2011.10.001

Topczewski, J., Sepich, D. S., Myers, D. C., Walker, C., Amores, A., Lele, Z., Hammerschmidt, M., Postlethwait, J. and Solnica-Krezel, L. (2001). The zebrafish glypican knypek controls cell polarity during gastrulation movements of convergent extension. *Dev. Cell* **1**, 251-264. doi:10.1016/S1534-5807(01)00005-3

Townley, R. A. and Bülow, H. E. (2011). Genetic analysis of the heparan modification network in Caenorhabditis elegans. *J. Biol. Chem.* **286**, 16824-16831. doi:10.1074/jbc.M111.227926

Tsuda, M., Kamimura, K., Nakato, H., Archer, M., Staatz, W., Fox, B., Humphrey, M., Olson, S., Futch, T., Kaluza, V. et al. (1999). The cell-surface proteoglycan Dally regulates Wingless signalling in Drosophila. *Nature* **400**, 276-280. doi:10.1038/22336

Tukachinsky, H., Lopez, L. V. and Salic, A. (2010). A mechanism for vertebrate Hedgehog signaling: recruitment to cilia and dissociation of SuFu-Gli protein complexes. *J. Cell Biol.* **191**, 415-428. doi:10.1083/jcb.201004108

Tukachinsky, H., Petrov, K., Watanabe, M. and Salic, A. (2016). Mechanism of inhibition of the tumor suppressor Patched by Sonic Hedgehog. *Proc. Natl. Acad. Sci. USA* **113**, E5866-E5875. doi:10.1073/pnas.1606719113

Turnbull, J. E., Fernig, D. G., Ke, Y., Wilkinson, M. C. and Gallagher, J. T. (1992). Identification of the basic fibroblast growth factor binding sequence in fibroblast heparan sulfate. *J. Biol. Chem.* **267**, 10337-10341. doi:10.1016/S0021-9258(19)50023-0

Vuillaume, M.-L., Moizard, M.-P., Rossignol, S., Cottereau, E., Vonwill, S., Alessandri, J.-L., Busa, T., Colin, E., Gérard, M., Giuliano, F. et al. (2018). Mutation update for the GPC3 gene involved in Simpson-Golabi-Behmel syndrome and review of the literature. *Hum. Mutat.* **39**, 790-805. doi:10.1002/humu.23428

Wen, X., Lai, C. K., Evangelista, M., Hongo, J.-A., de Sauvage, F. J. and Scales, S. J. (2010). Kinetics of hedgehog-dependent full-length Gli3 accumulation in primary cilia and subsequent degradation. *Mol. Cell. Biol.* **30**, 1910-1922. doi:10.1128/MCB.01089-09

Wierbowski, B. M., Petrov, K., Aravena, L., Gu, G., Xu, Y. and Salic, A. (2020). Hedgehog pathway activation requires coreceptor-catalyzed, lipid-dependent relay of the Sonic Hedgehog ligand. *Dev. Cell* **55**, 450-467.e58. doi:10.1016/j.devcel.2020.09.017

Williams, E. H., Pappano, W. N., Saunders, A. M., Kim, M.-S., Leahy, D. J. and Beachy, P. A. (2010). Dally-like core protein and its mammalian homologues mediate stimulatory and inhibitory effects on Hedgehog signal response. *Proc. Natl. Acad. Sci. USA* **107**, 5869-5874. doi:10.1073/pnas.1001777107

Wilson, N. H. and Stoeckli, E. T. (2013). Sonic hedgehog regulates its own receptor on postcrossing commissural axons in a glypican1-dependent manner. *Neuron* **79**, 478-491. doi:10.1016/j.neuron.2013.05.025

Witt, R. M., Hecht, M.-L., Pazyra-Murphy, M. F., Cohen, S. M., Noti, C., van Kuppevelt, T. H., Fuller, M., Chan, J. A., Hopwood, J. J., Seeberger, P. H. et al. (2013). Heparan sulfate proteoglycans containing a glypican 5 core

and 2-O-sulfo-iduronic acid function as Sonic Hedgehog co-receptors to promote proliferation. *J. Biol. Chem.* **288**, 26275-26288. doi:10.1074/jbc.M112.438937

Xu, D. and Esko, J. D. (2014). Demystifying heparan sulfate-protein interactions. *Annu. Rev. Biochem.* **83**, 129-157. doi:10.1146/annurev-biochem-060713-035314

Yan, D. and Lin, X. (2007). Drosophila glypican Dally-like acts in FGF-receiving cells to modulate FGF signaling during tracheal morphogenesis. *Dev. Biol.* **312**, 203-216. doi:10.1016/j.ydbio.2007.09.015

Yao, S., Lum, L. and Beachy, P. (2006). The ihog cell-surface proteins bind Hedgehog and mediate pathway activation. *Cell* **125**, 343-357. doi:10.1016/j.cell.2006.02.040

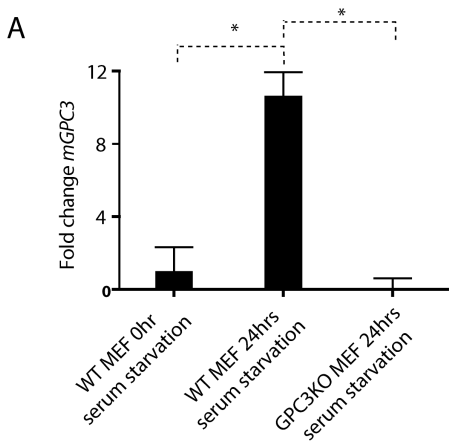
A
*
*
12
8
4
0
Fold change mGPC3
WT MEF 0hr serum starvation
WT MEF 24hrs serum starvation
GPC3KO MEF 24hrs serum starvation

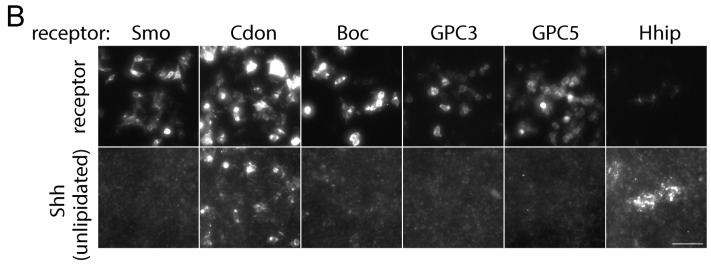
B
receptor:
Smo
Cdon
Boc
GPC3
GPC5
Hhip
receptor
Shh (unlipidated)

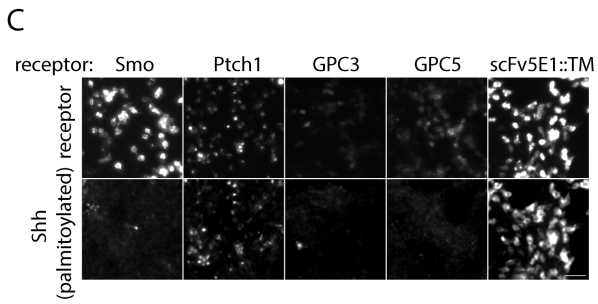
C
receptor:
Smo
Ptch1
GPC3
GPC5
scFv5E1::TM
receptor
Shh (palmitoylated)

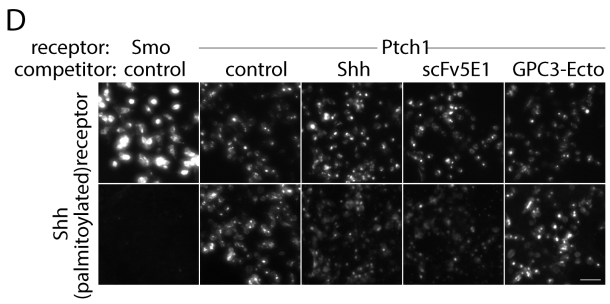
D
receptor:
Smo
Ptch1
competitor:
control
control
Shh
scFv5E1
GPC3-Ecto
Shh (palmitoylated)
receptor

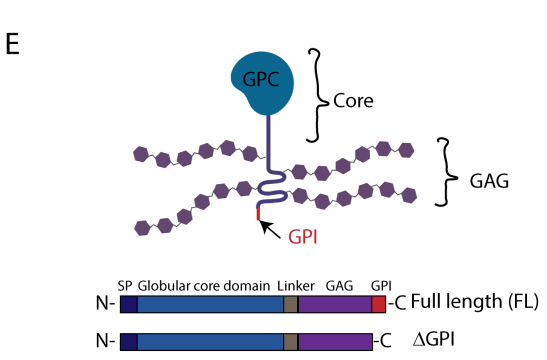
E
GPC
Core
GAG
GPI
SP
Globular core domain
Linker
GAG
GPI
N-
-C Full length (FL)
N-
-C
ΔGPI

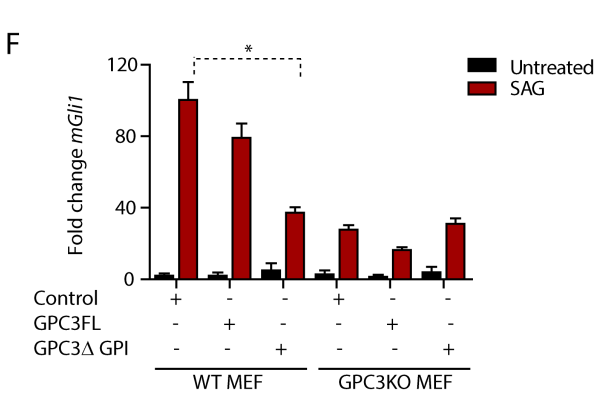
F
*
120
80
40
0
Fold change mGli1
Untreated
SAG
Control
GPC3FL
GPC3Δ GPI
WT MEF
GPC3KO MEF

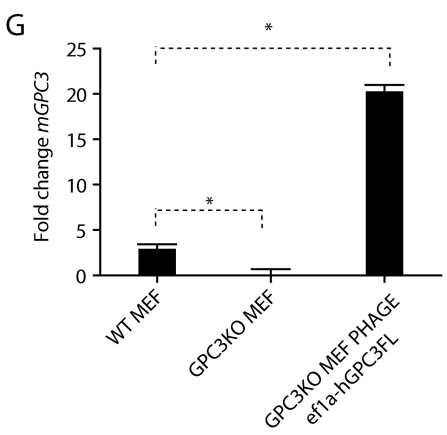
G
*
*
25
20
15
10
5
0
Fold change mGPC3
WT MEF
GPC3KO MEF
GPC3KO MEF PHAGE ef1a-hGPC3FL

Fig. S1. Related to Figure 1

(A) WT or *Gpc3*^{KO} MEFs were serum-starved for the indicated time, and levels of *mGPC3* transcript were measured by qRT-PCR. Bars show average fold-change for three replicates, and error bars show SEM. * denotes statistical significance, $p<0.05$. *mGPC3* transcripts are present in WT, but not *Gpc3*^{KO}, MEFs. Serum starvation increases *mGPC3* transcript levels.

(B) Representative fluorescence micrographs for the experiment quantified in Figure 1B, showing expression of eGFP-tagged receptors (top) and corresponding binding of AlexaFluor 594–labeled unlipidated Shh (bottom). Scale bar = 50μm.

(C) As in (B), but for the experiment quantified in Figure 1C, showing binding of TMR-labeled palmitoylated Shh (bottom). Scale bar = 50μm.

(D) As in (C), but for the experiment quantified in Figure 1D. Scale bar = 50μm.

(E) Cartoon representation of full length (FL) and ΔGPI GPC3 constructs.

(F) WT or *Gpc3*^{KO} MEFs, transduced with constructs expressing GPC3 FL or GPC3 ΔGPI, were incubated with SAG (1μM) or control media for 24 hours, and Hh signaling was measured by qRT-PCR for *Gli1*. GPC3ΔGPI expression inhibits Hh signaling in WT cells. Bars show average fold-change for three replicates, and error bars show SEM. * denotes statistical significance, $p<0.05$.

(G) *mGPC3* transcript levels were measured by qRT-PCR in WT MEFs, *Gpc3*^{KO} MEFs, and *Gpc3*^{KO} MEFs transduced with a lentivirus expressing GPC3 FL. Bars show average fold-change for three replicates, and error bars show SEM. * denotes statistical significance, $p<0.05$.

Journal of Cell Science • Supplementary information

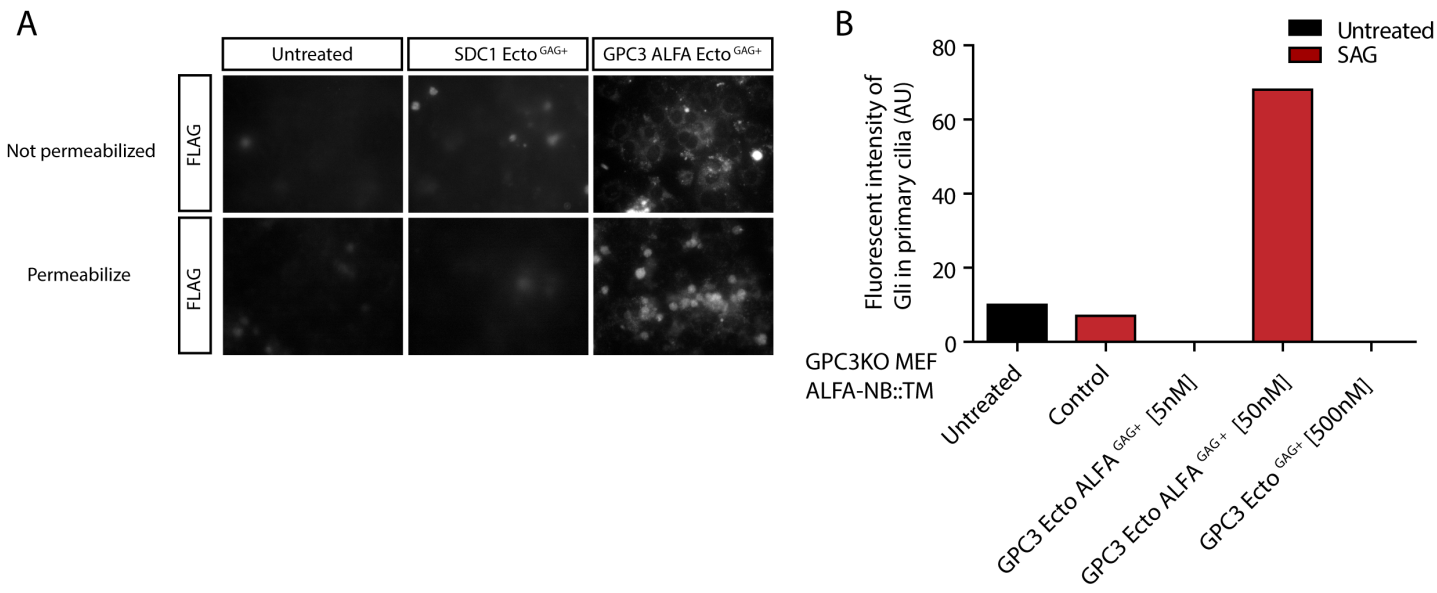

Fig. S2. Related to Figure 2.

(A) *Gpc3*^{KO} MEFs expressing ALFA-NB::TM were incubated for 24 hours with 50 nM FLAG-tagged GPC3-ALFA-Ecto^{GAG+} or SDC1-Ecto^{GAG+} (negative control), followed by anti-FLAG immunofluorescence microscopy, with or without permeabilization with 1% Triton X-100. GPC3-ALFA-Ecto^{GAG+} is recruited to cells expressing ALFA-NB::TM.

(B) *Gpc3*^{KO} MEFs expressing ALFA-NB::TM were incubated with SAG (1μM), in the presence of the indicated concentrations of purified GPC3-Ecto-ALFA^{GAG+} for 6hrs. Ciliary intensity of endogenous Gli protein was measured by immunofluorescence microscopy. 100-150 cilia were measured per condition. While 50 nM GPC3-Ecto-ALFA^{GAG+} rescues Gli recruitment to cilia, 500 nM GPC3-Ecto-ALFA^{GAG+} is inhibitory.

Journal of Cell Science • Supplementary information

A

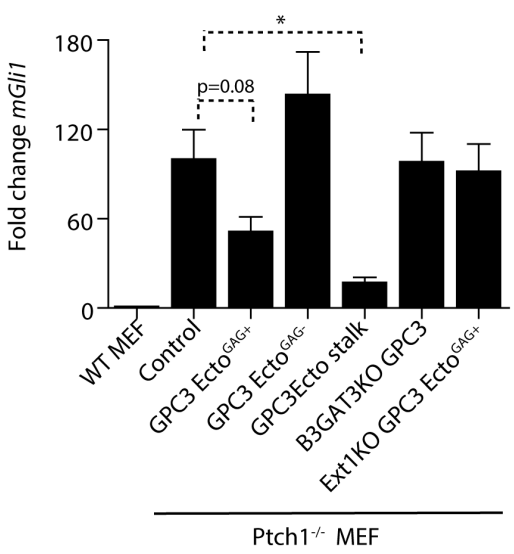
Fold change mGli1
180
120
60
0
*
p=0.08
WT MEF
Control
GPC3 Ecto GAG+
GPC3 Ecto GAG-
GPC3Ecto stalk
B3GAT3KO GPC3
Ext1KO GPC3 Ecto GAG+
Ptch1-/- MEF

B

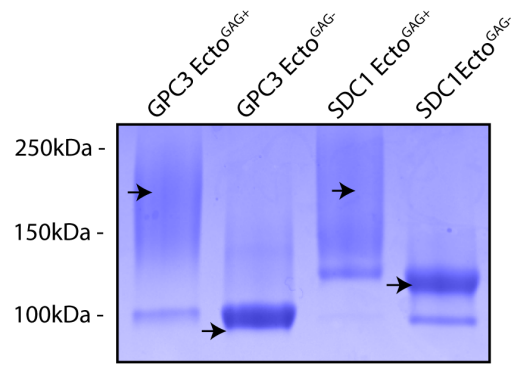
GPC3 Ecto GAG+
GPC3 Ecto GAG-
SDC1 Ecto GAG+
SDC1Ecto GAG-
250kDa -
150kDa -
100kDa -

C

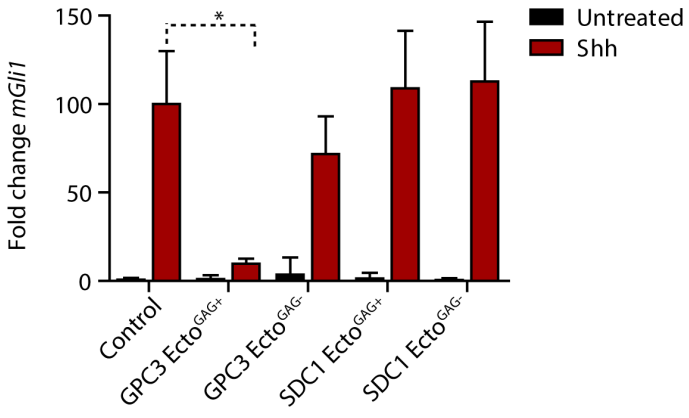
Fold change mGli1
150
100
50
0
*
Untreated
Shh
Control
GPC3 Ecto GAG+
GPC3 Ecto GAG-
SDC1 Ecto GAG+
SDC1 Ecto GAG-

D

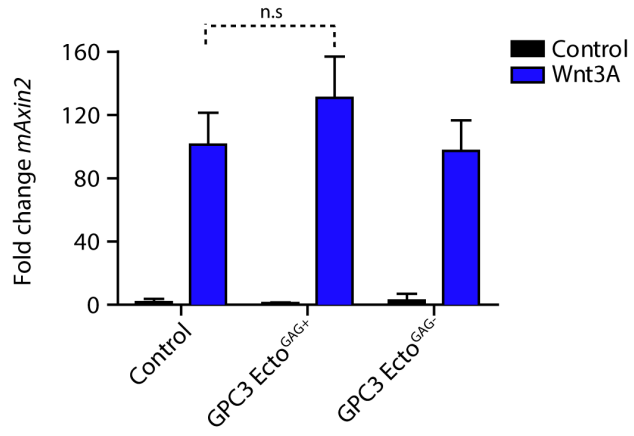
Fold change mAxin2
160
120
80
40
0
n.s
Control
Wnt3A
Control
GPC3 Ecto GAG+
GPC3 Ecto GAG-

Fig. S3. Related to Figure 3

(A) *Ptch1*$^{-/-}$ MEF cells were incubated with the indicated purified proteins (1μM) for 24 hours, and Hh pathway activity was measured by qRT-PCR for *Gli1*. HS-modified GPC3-Ecto and stalk domain antagonize constitutive Hh pathway activation. GPC3-Ecto proteins purified from *EXT1*^{KO} or from *B3GAT3*^{KO} cells (CS-modified and unmodified, respectively) are inactive. Bars show average fold-change for three replicates, and error bars show SEM. * denotes statistical significance, $p<0.05$.

(B) GPC3-Ecto and SDC1-Ecto fused to HaloTag were expressed in HEK293T cells and were affinity purified from conditioned media. The proteins were then separated by size-exclusion chromatography, to isolate GAG-modified and GAG-unmodified fractions, which were analyzed by SDS-PAGE and Coomassie staining. Arrows indicate relevant protein species in each gel lane.

(C) WT MEFs were incubated with Shh or control media for 24 hours, in the absence or presence of the indicated purified proteins (1μM). Hh signaling was measured by qRT-PCR for *Gli1*. SDC1-Ecto has no effect on Hh signaling, while GPC3-Ecto inhibits signaling in a GAG-dependent manner. Bars show average fold-change for three replicates, and error bars show SEM. * denotes statistical significance, $p<0.05$.

(D) As in (C), but with Wnt3A treatment and assaying Wnt pathway activation by qRT-PCR for *Axin2.* GAG-modified and unmodified GPC3-Ecto has no effect on Wnt signaling. Bars show average fold-change for three replicates, and error bars show SEM. * denotes statistical significance, $p<0.05$.

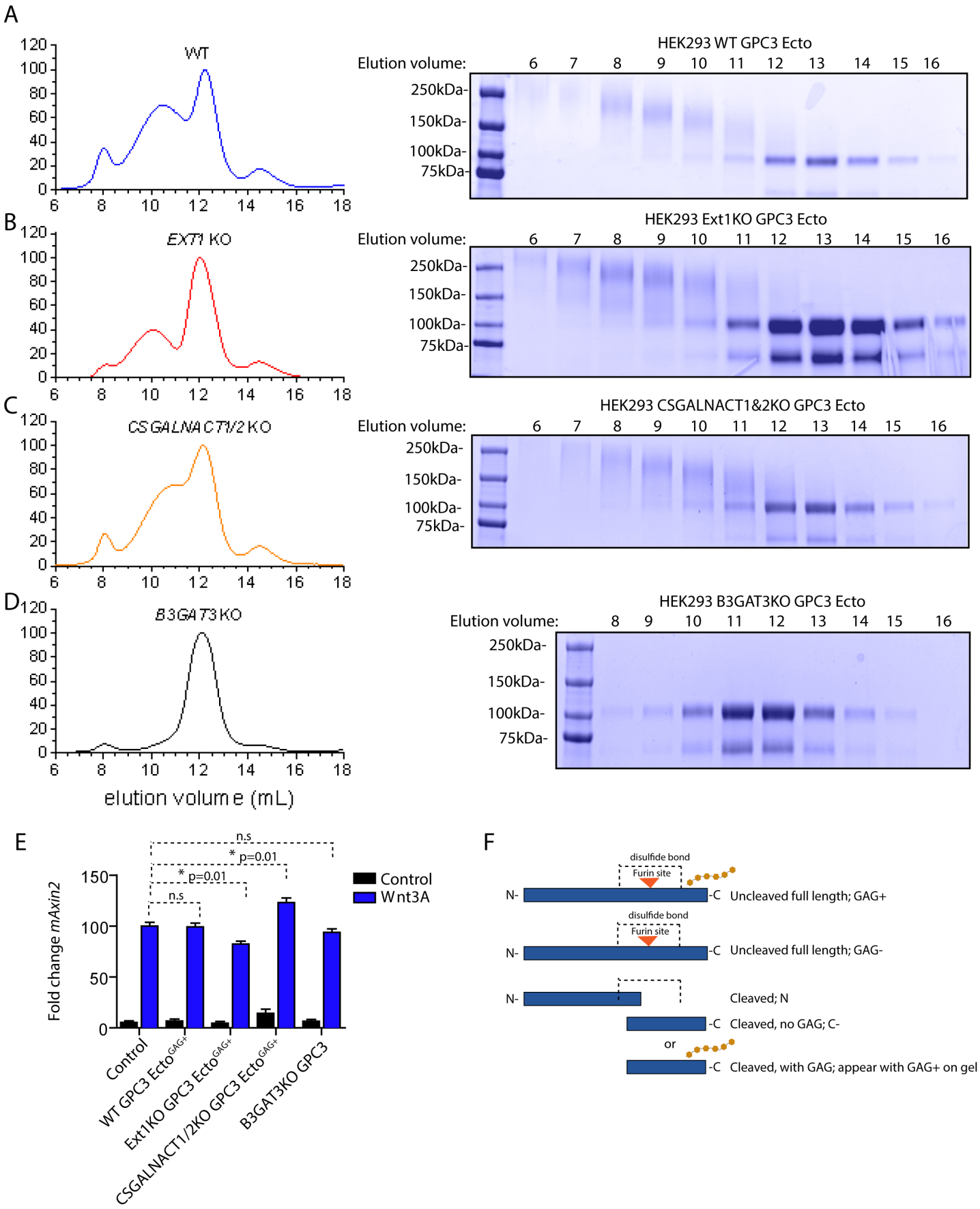

Journal of Cell Science • Supplementary information

Fig. S4. Related to Figure 4

(A) UV trace for size exclusion chromatography of GPC3-Ecto, affinity-purified from media conditioned by WT HEK293T cells (left). The indicated fractions were analyzed by SDS-PAGE and Coomassie staining (right).

(B) As in (A), but with GPC3-Ecto secreted by *Ext1*^{KO} cells.

(C) As in (A), but with GPC3-Ecto secreted by *CSGALNACT1,2*^{KO} cells.

(D) As in (A), but with GPC3-Ecto secreted by *B3GAT3*^{KO} cells.

(E) WT MEFs were incubated with Wnt3A or control media for 24 hours, in the absence or presence of GPC3-Ecto proteins (1μM), expressed and purified from the indicated cells. Wnt signaling was measured by qRT-PCR for *Axin2*. Bars show average fold-change for three replicates, and error bars show SEM. * denotes statistical significance, $p<0.05$. n.s =$p>0.05$.

(F) Cartoon representation of GPC3 cleavage by Furin, related to Figure 4B.

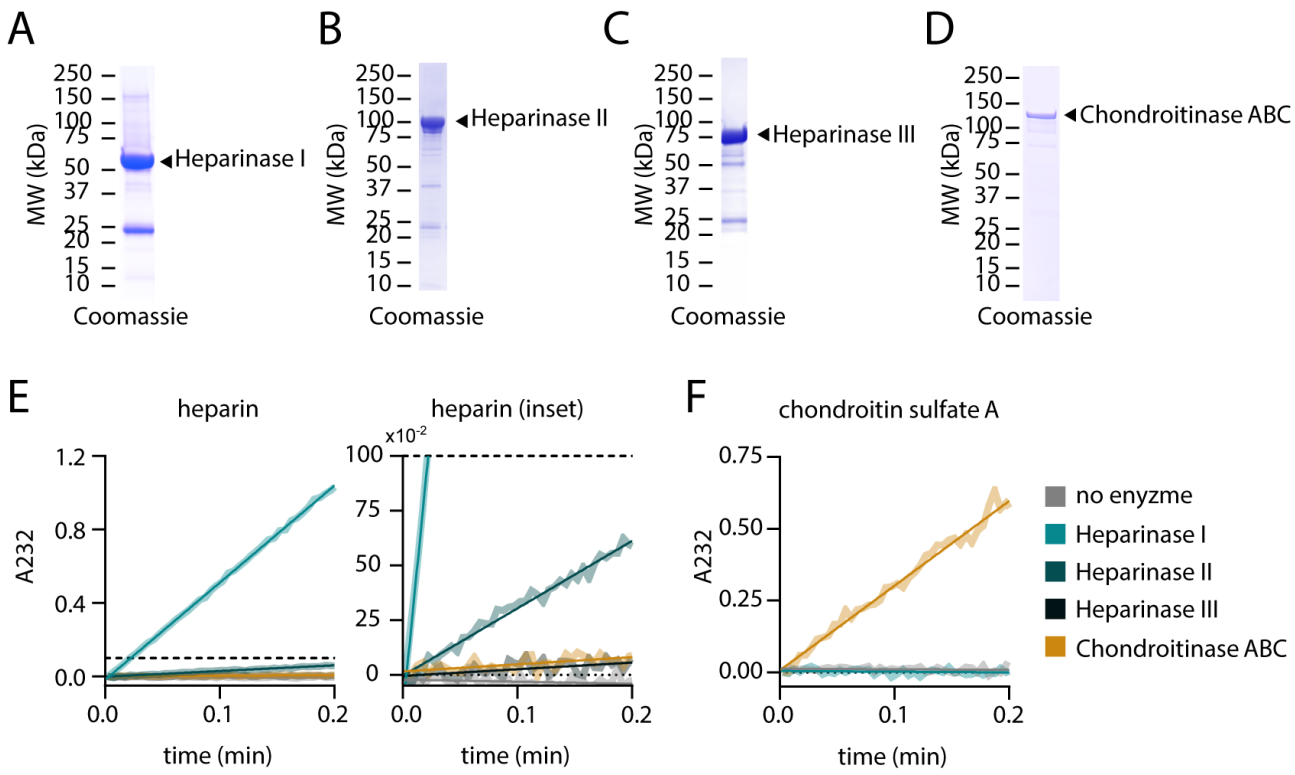

Fig. S5. Related to Materials and Methods

(A) GST-tagged *B. thetaiotaomicron* heparinase I (*bt4675*) was purified by glutathione affinity chromatography followed by gel filtration on a Superdex 200 26/60 column. Protein species well separated from the void volume were pooled, concentrated, and analyzed by SDS-PAGE and Coomassie staining.

(B) As in (A), but for *B. thetaiotaomicron* heparinase II (*bt4652*).

(C) As in (A), but for *B. thetaiotaomicron* heparinase III (*bt4657*).

(D) As in (A), but for *B. thetaiotaomicron* chondroitinase ABC (*bt3350*).

(E) Purified recombinant enzymes (20 μg) from (A)-(D) were incubated with 1 mg/mL porcine intestinal heparin in a total volume of 1 mL, and liberation of unsaturated non-reducing ends was quantified over time by continuous measurement at A232. Data (thick, light line) are fit with a linear regression (thin, dark line), used to calculate the specific activities reported in Table S4. Heparinase I (left) and heparinase II (see inset, right) act on heparin. Heparinase III, which acts on less highly sulfated HS substrates, and chondroitinase ABC are inactive against the heparin substrate.

(F) As in (E), except assaying enzyme activity on chondroitin sulfate A. Only chondroitinase ABC exhibits activity in this assay.

Journal of Cell Science • Supplementary information

Table S1. Generation of null cell lines by CRISPR-Cas9

Target Gene	gRNA #	NCBI Reference Sequence	Target Site Description	gRNA Sequence	gRNA Orientation	Associated Plasmid	Associated Cell Line
B3GAT3	1	NM_012200	Exon 3	TTCCGCTGCTCGACACCACG	antisense	pBMW673	BMW170.41
EXT1	1	NM_000127	Exon 1	GCCAGAAATGATCCGGACTG	antisense	pBMW606	BMW171.17
CSGALNACT1	1	NM_001130518	Exon 4	GGGTGCAGGCCAACATGTAC	antisense	pBMW703	BMW301.16
CSGALNACT2	1	NM_018590	Exon 2	GCCAAACTACCCAGTGAGTA	sense	pBMW704	BMW301.16
Gpc3	1	NM_016697	Exon 2	TGAGTTCCATACTCGCAGAC	antisense	pYCL1	YCL1.24
Gpc3	2	NM_016697	Exon 3	TGCGGTGGTTATTGCAATGT	sense	pYCL2	YCL1.24

Target Gene	gRNA #	Direction	Barcode Sequence	Target Recognition Sequence
B3GAT3	1	Forward	ACACTCTTTCCCTACACGACGCTCTTCCGATCT	CCTCCTCTTCACACACCTGG
B3GAT3	1	Reverse	GTGACTGGAGTTCAGACGTGTGCTCTTCCGATCT	CAAAGTAGACGACTCCTTGGGT
EXT1	1	Forward	ACACTCTTTCCCTACACGACGCTCTTCCGATCT	TTGTCTCGCCCTTTTGTTTTAT
EXT1	1	Reverse	GTGACTGGAGTTCAGACGTGTGCTCTTCCGATCT	AAATGTGCACGCTGGAATC
CSGALNACT1	1	Forward	ACACTCTTTCCCTACACGACGCTCTTCCGATCT	TTCCTGAATGATGATGGTTCG
CSGALNACT1	1	Reverse	GTGACTGGAGTTCAGACGTGTGCTCTTCCGATCT	TGGTACCCCTCCTTCCCC
CSGALNACT2	1	Forward	ACACTCTTTCCCTACACGACGCTCTTCCGATCT	ACAAAGAGCAAGCACCTAGTGA
CSGALNACT2	1	Reverse	GTGACTGGAGTTCAGACGTGTGCTCTTCCGATCT	CTTTTCTTCAGGATGGCGAGT
Gpc3	1	Forward	ACACTCTTTCCCTACACGACGCTCTTCCGATCT	CAACATGCTGCTCAAGAAAGAT
Gpc3	1	Reverse	GTGACTGGAGTTCAGACGTGTGCTCTTCCGATCT	GCCATTGAACAGTACATCGAAA
Gpc3	2	Forward	ACACTCTTTCCCTACACGACGCTCTTCCGATCT	ACACTACCGACCACCTCAAGTT
Gpc3	2	Reverse	GTGACTGGAGTTCAGACGTGTGCTCTTCCGATCT	TACTTGTCGATCTCCACCACAC

gRNA #	Allele 1 Sequence	Allele 1 Type	Allele 1 % Aligned Reads	Allele 2 Sequence	Allele 2 Type	Allele 2 % Aligned Reads	Allele 3 Sequence	Allele 3 Type	Allele 3 % Aligned Reads
1	AGCCTGGCTG//TGGGTGGGGA	68-nt deletion	51%	CGTG-TGTCGAGCAGCGGAA	1-nt deletion	26%	CGTGG(G)TGTCGAGCAGCGGAA	1-nt insertion	23%
1	GCACCACCCC//CCGCTTCCCG	20-nt deletion	92%	GGCTTGCACC//[CCC]CCCCGCTTCC	20-nt deletion / 3-nt mutation	8%	--	--	--
1	CTGTGCTATC//ACTGCCCAGG	53-nt deletion	74%	GTA--TGTTGGCCTGCACCC	2-nt deletion	26%	--	--	--
1	GCCAAACTACCCAGTGA(A)GTA	1-nt insertion	100%	--	--	--	--	--	--
1	GTCTGCGAGTATGGACTCA	wild-type	72%	GT----------GGAACTCA	10-nt deletion	28%	--	--	--
2	TGCG-TGGTTATTGCAATGT	1-nt deletion	35%	TGCGG(G)TGGTTATTGCAATGT	1-nt insertion	30%	TGCGGT---TATTGCAATGT	3-nt deletion	35%

Journal of Cell Science • Supplementary information

Table S2. List of expression constructs

pBMW Identifier	Vector	Promoter	Short Name	Full Transgene	Eukaryotic Resistance Marker	Bacterial Resistance Marker	Category	Subcategory	Reference
pBMW673	pX459	U6	*B3GAT3*^{KO}	hB3GAT3_CRISPR_KO_gRNA1	Puro	Amp	CRISPR knockout	GAG biosynthesis	this paper
pBMW606	pX459	U6	*EXT1*^{KO}	hEXT1_CRISPR_KO_gRNA1	Puro	Amp	CRISPR knockout	GAG biosynthesis	this paper
pBMW703	pX459	U6	*CSGALNACT1*^{KO}	hCSGALNACT1_CRISPR_KO_gRNA1	Puro	Amp	CRISPR knockout	GAG biosynthesis	this paper
pBMW704	pX459	U6	*CSGALNACT2*^{KO}	hCSGALNACT2_CRISPR_KO_gRNA1	Puro	Amp	CRISPR knockout	GAG biosynthesis	this paper
pYCL1	pX459	U6	*Gpc3*^{KO}	mGpc3_CRISPR_KO_gRNA1	Puro	Amp	CRISPR knockout	*Gpc3*^{KO}	this paper
pYCL2	pX459	U6	*Gpc3*^{KO}	mGpc3_CRISPR_KO_gRNA2	Puro	Amp	CRISPR knockout	*Gpc3*^{KO}	this paper
pAS63	pCS2	IE94-CMV	Smo	mSMO-FL::fTEV-EGFP	--	Amp	binding experiments	negative control	Wierbowski et al., 2020
pAS58	pHAGE2	CAG-CMV	Ptch1	mPTCH1-Del(C)Tail::fEGFP	Blast	Amp	binding experiments	positive control	Wierbowski et al., 2020
pBMW177	pHAGE2	CAG-CMV	Cdon	hCDON-Del(C)TM1::hCDON-Del(N)FNs::fTEV-EGFP	Blast	Amp	binding experiments	positive control	Wierbowski et al., 2020
pBMW281	pCS2	IE94-CMV	Boc	hBOC-Del(C)TM1::hBOC-Del(N)FNs::fTEV-EGFP	--	Amp	binding experiments	positive control	Wierbowski et al., 2020
pBMW241	pCS2	IE94-CMV	Hhip	EGFPf::hHHIP-FL	--	Amp	binding experiments	positive control	this paper
pBMW304	pHAGE2	CAG-CMV	scFv5E1::TM	scFv5E1-LH::hCDON-Del(N)FNs::fTEV-EGFP	Blast	Amp	binding experiments	positive control	Wierbowski et al., 2020; Maun et al., 2010
pBMW243	pCS2	IE94-CMV	GPC3	EGFPf::mGPC3-FL	--	Amp	binding experiments	experimental sample	this paper
pBMW244	pCS2	IE94-CMV	GPC5	EGFPf::hGPC5-FL	--	Amp	binding experiments	experimental sample	this paper
pAS295	pHAGE2	CAG-CMV	ALFA-NB::TM	HPC-NbALFA::hCDON-TM-CTD	Blast	Amp	stable mammalian expression	ALFA-NB recruitment system	Wierbowski et al., 2020; Gotzke et al., 2019
pAS283	pHAGE2	CAG-CMV	GPC3	FLAG-mGPC3-FL	Blast	Amp	stable mammalian expression	*Gpc3*^{KO} rescue	this paper
pAS173	pHAGE2	CAG-CMV	GPC3-Ecto	FLAG-HT7-PreSci::mGPC3-Del(C)GPI	Blast	Amp	stable mammali	*Gpc3*^{KO} rescue	this paper

							an expression		
pAS272	pTWIN	T7lac	unlipidated Shh	SHH(C24A)-N	--	Amp	bacterial protein production	Shh ligand for binding experiments; competitor for Ptch1 interaction	Wierbowski et al., 2020
pBMW643	pGEX-2TK	Ptac	Heparinase I	GST-Thromb::B.theta.HeparinaseI	--	Amp	bacterial protein production	heparinases	this paper
pBMW644	pGEX-2TK	Ptac	Heparinase II	GST-Thromb::B.theta.HeparinaseII	--	Amp	bacterial protein production	heparinases	this paper
pBMW645	pGEX-2TK	Ptac	Heparinase III	GST-Thromb::B.theta.HeparinaseIII	--	Amp	bacterial protein production	heparinases	this paper
pBMW678	pGEX-2TK	Ptac	Chondroitinase ABC	GST-Thromb::B.theta.ChondroitinaseABC	--	Amp	bacterial protein production	chondroitinase	this paper
pAS48	pCS2	IE94-CMV	Shh	hSHH-N	--	Amp	transient mammalian protein production	Shh conditioned medium production	Wierbowski et al., 2020
pAS75	pCS2	IE94-CMV	palmitoylated Shh	hSHH-N::fHT7-PreSci-HPC	--	Amp	transient mammalian protein production	Shh ligand for binding experiments	Wierbowski et al., 2020
pBMW814	pHAGE2	CAG-CMV	scFv5E1	scFv5E1::PreSci-fHT7-HPC	Blast	Amp	stable mammalian protein production	competitor for Ptch1 interaction	Wierbowski et al., 2020
pAS290	pHAGE2	CAG-CMV	GPC3-Ecto-ALFA	FLAG-mGPC3-Ecto-ALFA	Blast	Amp	stable mammalian protein production	ALFA-NB recruitment system	this paper
pBMW637	pHAGE2	CAG-CMV	SDC1-Ecto	hSDC1-Ecto::PreSci-fHT7-HPC	Blast	Amp	stable mammalian protein production	negative control	this paper
pAS174	pHAGE2	CAG-CMV	GPC3-Ecto	mGPC3-Del(C)GPI::fHT7-PreSci-HPC	Blast	Amp	stable mammalian protein production	experimental sample	this paper
pBMW697	pHAGE2	CAG-CMV	GPC3-Ecto^{PreScission}	FLAG-mGPC3-Core::PreSci::mGPC3-Stalk::fHT7-HPC	Blast	Amp	stable mammalian protein production	cleavable GPC3-Ecto	this paper
pBMW675	pHAGE2	CAG-CMV	GPC3-Stalk	HPC-HT7-PreSci::mGPC3-Stalk	Blast	Amp	stable mammalian protein production	stalk sufficiency test	this paper

pBMW554	pHAGE2	CAG-CMV	GPC1-Ecto	hGPC1-Del(C)GPI::fHT7-PreSci-HPC	Blast	Amp	stable mammalian protein production	core necessity test	this paper
pBMW555	pHAGE2	CAG-CMV	GPC2-Ecto	hGPC2-Del(C)GPI::fHT7-PreSci-HPC	Blast	Amp	stable mammalian protein production	core necessity test	this paper
pBMW833	pHAGE2	CAG-CMV	$GPC1^{core}$-$GPC3^{stalk}$-Ecto	hGPC1-Core::mGPC3-Stalk::fHT7-PreSci-HPC	Blast	Amp	stable mammalian protein production	core necessity test	this paper
pBMW834	pHAGE2	CAG-CMV	$GPC3^{core}$-$GPC1^{stalk}$-Ecto	mGPC3-Core::hGPC1-Stalk::fHT7-PreSci-HPC	Blast	Amp	stable mammalian protein production	core necessity test	this paper
pBMW817	pHAGE2	CAG-CMV	$GPC2^{core}$-$GPC3^{stalk}$-Ecto	hGPC2-Core::mGPC3-Stalk::fHT7-PreSci-HPC	Blast	Amp	stable mammalian protein production	core necessity test	this paper
pBMW818	pHAGE2	CAG-CMV	$GPC3^{core}$-$GPC2^{stalk}$-Ecto	mGPC3-Core::hGPC2-Stalk::fHT7-PreSci-HPC	Blast	Amp	stable mammalian protein production	core necessity test	this paper

Table S3. List of qRT-PCR primers

Target	Forward qPCR Primer	Reverse qPCR Primer
mGli1	TACCATGAGCCCTTCTTTAGGA	GCATCATTGAACCCCGAGTAG
mCyclo	GGAGATGGCACAGGAGGAA	GCCCGTAGTGCTTCAGCTT
mAxin2	GCTCCAGAAGATCACAAAGAGC	AGCTTTGAGCCTTCAGCATC

Table S4. Specific activities of recombinant heparinases and chondroitinase

Gene	Protein	Substrate	Specific Activity (pmol/min/µg)
bt3350	*B. theta* Chondroitinase ABC	chondroitin sulfate A	38802.63
		heparin	*N.D.*
bt4675	*B. theta* Heparinase I	chondroitin sulfate A	*N.D.*
		heparin	69500.00
bt4652	*B. theta* Heparinase II	chondroitin sulfate A	*N.D.*
		heparin	4057.89
bt4657	*B. theta* Heparinase III	chondroitin sulfate A	*N.D.*
		heparin	*N.D.*